Theory of the Microscopic Maser Phase Transitions

Per K. Rekdal[1,a] and Bo-Sture K. Skagerstam[2,a,b]

[a] Department of Physics, The Norwegian University of Science and
Technology, N-7034 Trondheim, Norway

[b] Theory Division, CERN, CH-1211 Geneva 23, Switzerland

Abstract

Phase diagrams of the micromaser system are mapped out in terms of the physical parameters at hand like the atom cavity transit time τ, the atom-photon frequency detuning $\Delta\omega$, the number of thermal photons n_b and the probability a for a pump atom to be in its excited state. Critical fluctuations are studied in terms of correlation measurements on atoms having passed through the micromaser or on the microcavity photons themselves. At sufficiently large values of the detuning we find a "twinkling" mode of the micromaser system. Detailed properties of the trapping states are also presented.

[1]Email address: perr@phys.ntnu.no.
[2]Email address: boskag@phys.ntnu.no.

1 INTRODUCTION

There are few systems in physics which exhibit a rich structure of phase transitions that can be investigated under clean experimental conditions and which at the same time can be studied by exact theoretical methods. Recent developments in cavity quantum electrodynamics, and in particular the use of beams of highly excited Rydberg atoms and resonant microcavities, has opened up an avenue to study one class of such systems in great detail. The micromaser system, which is a remarkable experimental realization of the idealised system of a two-level atom interacting with a second-quantised single-mode electromagnetic field, provides us with such an example (for reviews and references see e.g. [1]). The microlaser [2] is the counterpart in the optical regime.

Many features of the micromaser are of general interest. It can, for example, be argued that the micromaser system is a very simple illustration of the conjectured topological origin of second-order phase transitions [3], as will be briefly discussed later in the present paper. Various aspects of stochastic resonance can, furthermore, be studied in this system [4]. The micromaser also illustrates a remarkable feature of non-linear dynamical systems: turning on randomness may lead to an increased signal-to-noise ratio [5, 6].

The basic theory of the micromaser system as developed in Refs.[7, 8], which is limited to the case $a = 1$ and $\Delta\omega = 0$ only, suggests the existence of various phase transitions in the large N limit. Here N is the number of atoms passing the cavity in a single photon decay time. A natural order parameter is then the average photon "density" $\langle n \rangle / N$, where $\langle n \rangle$ denotes the average photon number with respect to the stationary micromaser photon distribution. By making use of an approximative approach in terms of a Fokker-Planck equation, details of the various transitions were worked out, like tunnelling times between the various phases (see e.g. [7, 8]). An exact treatment, in the large N limit, of the micromaser phase structure and the corresponding critical fluctuations in terms of a conventional correlation function of either the atoms leaving the micromaser or the photons in the cavity has been given in Refs.[9], where deviations from the Fokker-Planck equation approach were reported. It is of great interest to notice that spontaneous jumps in $\langle n \rangle / N$ and large correlation lengths close to micromaser phase transitions have been observed experimentally [1, 10]. Most of the experimental and theoretical studies have, however, been limited to the case $a = 1$ and $\Delta\omega = 0$. It is the purpose of the present paper to study the phase structure of the micromaser system and extend the results of Refs.[9] to the general case with $a \neq 1$ and $\Delta\omega \neq 0$ using methods which are exact in the large N limit. As will be argued below, several new intriguing physical properties of the

2

micromaser system are then unfolded. A short presentation of the main results of this paper has appeared elsewhere [11].

The paper is organised as follows. In Section 2 the theoretical framework is outlined, and a rapidly convergent large N limit is derived for the stationary micromaser photon probability distribution. The phase structure is investigated in Section 3 and the order parameter $\langle x \rangle$ is discussed in more detail in Section 4. The correlation length is analyzed numerically in Section 5 as well as in terms of various approximation schemes. The results of extensive numerical investigations of trapping states are presented in Section 6. Final remarks are given in 7.

2 THE PROBABILITY DISTRIBUTION

The pump atoms, which enter the cavity, are assumed to be prepared in an incoherent statistical mixture, i.e. the initial density matrix ρ_A of the atoms is of the diagonal form

$$\rho_A = \begin{pmatrix} a & 0 \\ 0 & b \end{pmatrix} \quad , \tag{1}$$

where $a + b = 1$. This form of the atomic density matrix is not of the most general form, but it leads to the possibility of an exact analytical treatment provided the photon field density matrix also is diagonal, which from now on we assume. The rate R of the injected atoms is assumed to be high enough to pump up the cavity, i.e. $R > \gamma = 1/T_{cav}$, or $N > 1$ in terms of the dimensionless flux variable $N = R/\gamma$. Here T_{cav} is the decay time of the cavity and hence γ is the typical decay rate for photons in the cavity. Furthermore, let τ denote the atomic transit-time through the resonant photon cavity.

For our purposes the continuous time formulation of the micromaser system [12] is suitable as a theoretical framework. Each atom is assumed to have the same probability $R\,dt$ of arriving in an infinitesimal time interval dt, i.e. they are Poisson distributed. Provided the interaction with the radiation field of the cavity takes less time than this interval, i.e. if $\tau \ll dt$, we may consider the atomic transitions to be instantaneous. The vector p formed by the diagonal density matrix elements of the photon field then obeys the master equation [12, 9]

$$\frac{dp}{dt} = -\gamma L p \quad , \tag{2}$$

3

where

$$L = L_C - N(M - 1) \ .$$ (3)

Here L_C describes the damping of the cavity (see e.g. Ref. [13] for an excellent account), i.e.

$$(L_C)_{nm} = (n_b + 1)[n\delta_{n,m} - (n + 1)\delta_{n+1,m}] + n_b[(n + 1)\delta_{n,m} - n\delta_{n,m+1}] \ ,$$ (4)

and $M = M(+) + M(-)$ has its origin in the Jaynes-Cummings (JC) model [14, 9] where

$$M(+)_{nm} = bq_{n+1}\delta_{n+1,m} + a(1 - q_{n+1})\delta_{n,m} \ ,$$ (5)

and

$$M(-)_{nm} = aq_n\delta_{n,m+1} + b(1 - q_n)\delta_{n,m} \ .$$ (6)

We observe the unitarity constraints

$$\sum_{n=0}^{\infty} M_{nm} = 1 \ ,$$

$$\sum_{n=0}^{\infty} (L_C)_{nm} = 0 \ .$$ (7)

The stationary solution of Eq. (2) is well known [7, 12] and is given by

$$\bar{p}_n = \bar{p}_0 \prod_{m=1}^{n} \frac{n_b \, m + Naq_m}{(1 + n_b) \, m + Nbq_m} \ ,$$ (8)

where $q_m \equiv q(m/N)$ and

$$q(x) = \frac{x}{x + \Delta^2} \ \sin^2 \left(\theta\sqrt{x + \Delta^2} \right) \ .$$ (9)

Here we have defined the natural and dimensionless parameter

$$\Delta^2 = \delta^2/N \ ,$$ (10)

where

$$\delta = \Delta\omega/2g \ ,$$ (11)

4

since it is always this particular combination of $\Delta\omega$, N and g which is involved. g is the single-photon Rabi frequency at zero detuning of the JC model [14]. n_b is the initial mean value of thermal photons in the cavity. Furthermore, the probability is expressed in terms of the scaled dimensionless pump parameter $\theta = g\tau\sqrt{N}$. The overall constant $\bar{p}_0$ in Eq. (8) is determined by the normalisation condition

$$\sum_{n=0}^{\infty} \bar{p}_n = 1 \quad . \tag{12}$$

In passing, we observe that at thermal equilibrium, i.e. when

$$\frac{a}{b} = \frac{n_b}{1 + n_b} \quad , \tag{13}$$

the probability distribution in Eq. (8) is in fact, as it should be, a Planck distribution. This particular distribution depends only on n_b, which is the corresponding mean value photon number, i.e.

$$\langle n \rangle \equiv \sum_{n=0}^{\infty} n\bar{p}_n = n_b \quad . \tag{14}$$

If Eq. (13) is not fulfilled then $\bar{p}_n$ describes a stationary photon distribution which therefore can be far from thermal equilibrium.

2.1 Large N Expansion

The large N behaviour of the stationary photon probability distribution $\bar{p}_n$ as given by Eq. (8) is difficult to handle. In order to obtain an appropriate expression which is rapidly convergent in the large N limit, and which neatly expresses the various micromaser phases, we can make use of a Poisson summation technique [15]. It is then natural to define the scaled photon number variable x, defined by $x = n/N$. The stationary probability distribution Eq. (8) then takes the form

$$\bar{p}(x) = \bar{p}_0 \sqrt{\frac{w(x)}{w(0)}} \, e^{-NV(x)} \quad , \tag{15}$$

where

$$V(x) = \sum_{k=-\infty}^{\infty} V_k(x) \quad . \tag{16}$$

The effective potential $V(x)$ is expressed in terms of

$$V_k(x) = -\int_0^x d\nu \, \ln[\, w(\nu)\,] \, \cos(2\pi N k \nu) \quad, \tag{17}$$

where

$$w(x) = \frac{n_b \, x + a \, q(x)}{(1 + n_b) \, x + b \, q(x)} \quad. \tag{18}$$

In this expression for $w(x)$, $q(x)$ is given by Eq. (9). We stress that Eq. (15) is exact.

In the large N limit Eq. (15) can be substantially simplified since the $V_k(x)$-terms in Eq. (17) do not contribute in this limit for $k \neq 0$. It is therefore the nature of the global minima of $V_0(x)$ which determines the probability distribution and the micromaser phase structure, apart from the zeros of $w(x)$ which correspond to trapping states [16]-[20]. The physics of trapping states will be discussed in Section 6.

2.2 The Thermal Distribution

If the only global minimum of $V_0(x)$ occurs at $x = 0$, we can expand the effective potential $V_0(x)$ around the origin. A straightforward expansion of $V_0(x)$ then leads to

$$V_0(x) = x \ln \left[\frac{1 + n_b + b\theta_{eff}^2}{n_b + a\theta_{eff}^2} \right] + \mathcal{O}(x^2) \quad, \tag{19}$$

where we have defined an effective pump θ-parameter

$$\theta_{eff}^2 = \theta^2 \, \frac{\sin^2(\theta\Delta)}{(\theta\Delta)^2} \quad. \tag{20}$$

Eq. (19) leads to the following properly normalised thermal photon probablity distribution

$$\bar{p}_n = \frac{1 + (1 - 2a) \, \theta_{eff}^2}{1 + n_b + b\theta_{eff}^2} \left(\frac{n_b + a \, \theta_{eff}^2}{1 + n_b + b \, \theta_{eff}^2} \right)^n \quad, \tag{21}$$

which is convergent provided

$$\theta_{eff}^2 \, (2a - 1) < 1 \quad. \tag{22}$$

Eq. (21) is exact in the large N limit, and corresponds to an increase of the temperature in the cavity. If $a < 1/2 + \Delta^2/2$ the distribution Eq. (21) is therefore always valid. If

$\Delta = 0$ convergence requires that $\theta^2 (2a - 1) < 1$, i.e. θ has to be sufficiently small when $a > 1/2$. We find that Eq. (21) also can be used to compute expectation values for finite N, even though the accuracy then depends on the actual micromaser parameters. When the micromaser is described by the thermal distribution in Eq. (21), we say that the system is in the thermal phase.

2.3   The Gaussian Distribution

If, on the other hand, non-trivial saddle-points of $V_0(x)$ exist, Eq. (15) can be written in the form

$$\bar{p}(x) = \sum_j \bar{p}_j(x) \ , \tag{23}$$

where $\sum_j$ is a sum over all saddle-points corresponding to minima of $V_0(x)$, and where $\bar{p}_j(x)$ is $\bar{p}(x)$ for x close to the saddle-points $x = x_j$. The saddle-points, $x(\theta)$, are determined by $V_0'(x) = 0$, since, as noted above, the $V_k(x)$-terms in Eq. (17) for $k \neq 0$ do not contribute in the large N-limit. For a fixed a and Δ we then have

$$(2a - 1) \sin^2 \left(\theta \sqrt{x(\theta) + \Delta^2} \ \right) - (x(\theta) + \Delta^2) = 0 \ , \tag{24}$$

corresponding to $w(x(\theta)) = 1$. This equation is independent of n_b and has non-trivial solutions only when $a \geq 1/2 + \Delta^2/2$. It is clear that a, Δ and $x(\theta)$ at a saddle-point are restricted by the condition

$$x(\theta) + \Delta^2 \leq 2a - 1 \ , \tag{25}$$

for any θ. The saddle-points $x = x(\theta)$ can conveniently be parametrically represented in the form [9]

$$x(\phi) + \Delta^2 = (2a - 1) \sin^2 \phi \ , \tag{26}$$

$$\theta(\phi) = \frac{1}{\sqrt{2a - 1}} \frac{\phi}{|\sin \phi|} \ , \tag{27}$$

with

$$\phi \geq \phi_0 \equiv \arcsin(|\Delta|/\sqrt{2a - 1}) \ . \tag{28}$$

We define branches of ϕ, labelled by $k = 0, 1, 2, ...$ such that ϕ varies in the intervals

$$\phi_0 + k\pi \leq \phi \leq (k+1)\pi - \phi_0 \quad , \quad k = 0, 1, 2, ... \quad . \tag{29}$$

Except for the first branch $k = 0$, the saddle-points corresponding to each of these branches are double-valued, that is, there are at most two values of $x(\theta)$ for a given θ. The first branch $k = 0$ is single-valued.

For a given a, Δ and θ, let $x = x_j(a, \Delta, \theta) \equiv x_j$ be a saddle-point corresponding to a minimum of $V_0(x)$. The equilibrium distribution in the neighbourhood of this minimum value x_j is then given in the following Gaussian form

$$\bar{p}_j(x) = \frac{T_j}{\sqrt{2\pi N}} \, e^{-\frac{N}{2}V_0''(x_j)(x-x_j)^2} \quad . \tag{30}$$

Here T_j is determined by the normalisation condition for $\bar{p}(x)$, i.e

$$T_j = \frac{e^{-NV_0(x_j)}}{\sum_m e^{-NV_0(x_m)}/\sqrt{V_0''(x_m)}} \quad , \tag{31}$$

and where

$$V_0''(x) = \frac{(2a-1)^2}{a + n_b(2a-1)} \frac{q(x) - xq'(x)}{x^2} \quad . \tag{32}$$

For the given parameters, the sum in Eq. (31) is supposed to be taken over all saddle-points corresponding to a minimum of $V_0(x)$, i.e. all saddle-points corresponding to $V_0''(x) > 0$. If $x = x_j$ does not correspond to a global minimum for the effective potential $V_0(x)$, then T_j is exponentially small in the large N limit. If $x = x_j$ corresponds to one and only one global minimum, we can neglect all the terms in the sum in T_j but $m = j$, in which case T_j is reduced to $T_j = \sqrt{V_0''(x_j)}$. In the neighbourhood of such a global minimum x_j the probability distribution in Eq. (30) is therefore reduced to

$$\bar{p}_j(x) = \sqrt{\frac{V_0''(x_j)}{2\pi N}} \, e^{-\frac{N}{2}V_0''(x_j)(x-x_j)^2} \quad . \tag{33}$$

which is, strictly speaking, only valid in a sufficiently small neighbourhood of x_j.

However, since $\bar{p}_j(x)$ in Eq. (30) is exponentially small when x is not in the neighbourhood of x_j, the probability distribution for any x is given by

$$\bar{p}(x) = \sum_{j^*} \bar{p}_j(x) \quad , \tag{34}$$

8

where $\sum_{j*}$ denotes the sum over the global minima of $V_0(x)$ only. Hence, when there are several saddle-points, the actual maser phase is described by the saddle-points which correspond to the global minima of $V_0(x)$ only. In the next section, we will actually argue that, for a fixed a, Δ and θ, we can have at most two competing global minima in the large N limit, i.e. there can be at most two terms in the $\sum_{j*}$-sum in Eq. (34).

When the micromaser is described by a distribution like Eq. (33) the mean occupation number $\langle n \rangle$ is proportional to the pumping rate N (see Section 4). The cavity then acts as a maser, i.e. the system is in a maser phase.

3 THE PHASE DIAGRAM

The probability distribution Eq. (8) determines micromaser phases as a function of the physical parameters at hand. In this section we will map out phase diagrams in the a- and θ-parameter space for a given $n_b \neq 0$ and Δ. In general a phase diagram is then determined by mapping out the global minima of the effective potential $V_0(x)$.

By the substitution $\phi = \theta\sqrt{x + \Delta^2}$, the effective potential in Eq. (17) can be written in the form

$$V_0(x) = V_0(\phi, \theta) = -\frac{2}{\theta^2} \int_{\theta|\Delta|}^{\phi} d\chi\, \chi\, \ln[w(\chi, \theta)] \quad . \tag{35}$$

Here we have defined

$$w(\chi, \theta) = \frac{n_b + a\, q(\chi, \theta)}{1 + n_b + b\, q(\chi, \theta)} \quad , \tag{36}$$

and

$$q(\chi, \theta) = \theta^2\, \frac{\sin^2 \chi}{\chi^2} \quad . \tag{37}$$

In Eq. (35), the upper integration limit ϕ and the pump parameter θ may take on arbitrary values. However, by choosing $x(\phi)$ and $\theta(\phi)$ according to Eq. (26) and Eq. (27) the effective potential is always at an extremum. We then arrive at an effective multi-branched potential as given by $V_0(\phi) = V_0(\phi, \theta(\phi))$. For a given branch k, the variable ϕ is limited by Eq. (29).

9

If we regard $V_0(\phi)$ as a function of θ, each branch of $V_0(\theta) = V_0(\phi, \theta(\phi))$ is at most double-valued except for branch $k = 0$. One sub-branch then corresponds to a maximum $(V_0''(x(\phi)) < 0)$, which is swept out first as ϕ increases, and the other corresponds to a minimum $(V_0''(x(\phi)) > 0)$. Here the $V_0''(x(\phi))$ is explicitly given by

$$V_0''(x(\phi)) = \frac{1 - \phi \cot \phi}{\sin^2 \phi \, [a + n_b(2a - 1)]} \quad . \tag{38}$$

To reconstruct the actual value of $V_0(x)$ for the k:th minimum (maximum), we write $V_0(x) = V_0(\phi)$, evaluated for the sub-branch with $V_0''(x(\phi)) > 0$ $(V_0''(x(\phi)) < 0)$.

A convenient representation of $V_0(\phi)$ for the branch k (given a, n_b, Δ) is

$$V_0(\phi) = [a + n_b(2a - 1)] \, I(\phi) \quad , \tag{39}$$

where

$$I(\phi) \equiv \int_{\phi_0 + k\pi}^{\phi} d\chi \, \chi^4 \, \frac{\sin(2\chi) - 2\sin^2(\chi)/\chi}{\left[\chi^2 n_b + a \, \theta(\phi)^2 \sin^2 \chi\right] \left[\chi^2(1 + n_b) + b \, \theta(\phi)^2 \sin^2 \chi\right]} \quad . \tag{40}$$

Here the upper integration limit ϕ has to be chosen according to Eq. (29). We notice the characteristic pre-factor $a + n_b(2a - 1)$ in Eq. (39) which actually determines the typical dependence of the parameters a and n_b at a saddle-point.

3.1   The Critical Parameters θ_0^* and θ_k

As a function of θ, the first extremum of $V_0(x)$ occurs at $\theta_0^* \equiv \theta(\phi_0)$, where ϕ_0 is given by Eq. (28). The critical pump parameter $\theta_0^* = \theta_0^*(a, \Delta)$ is therefore given by

$$\theta_0^* = \frac{\arcsin(|\Delta|/\sqrt{2a - 1})}{|\Delta|} \quad , \tag{41}$$

which is equivalent to

$$a = \frac{1}{2} + \frac{\Delta^2}{2\sin^2(\theta_0^* \Delta)} \quad . \tag{42}$$

When the system is not detuned, i.e. when $\Delta = 0$, this equation reduces to

$$a = \frac{1}{2} + \frac{1}{2(\theta_0^*)^2} \quad . \tag{43}$$

Eq. (41) determines the first thermal-maser critical line in the a- and θ- phase diagram. In the maser phase, the order parameter $\langle x \rangle = \langle n \rangle / N$ approaches zero when θ approaches $\theta_0^*(a, \Delta)$. Furthermore, in the large N limit, $\langle x \rangle$ is always zero in the thermal phase (see Section 4). Hence, the order parameter is continuous on this critical line. The first derivative of $\langle x \rangle$ with respect to θ is, however, discontinuous. In the maser phase we actually have

$$\frac{d\langle x \rangle}{d\theta} = 2(\sqrt{2a - 1})^3 \frac{\sin^3 \phi}{\tan \phi - \phi} \quad , \tag{44}$$

with $\phi \geq \phi_0$. When approaching the critical line from the maser phase, we see from Eq. (44) that $d\langle x \rangle / d\theta$ is non-zero (except for $a = 1/2$). The first thermal-maser critical line therefore corresponds to a line of second-order phase transitions.

In passing, we mention that in a topological analysis of the second-order phase transitions [3] of the micromaser system, $V_0(x)$ will play the role of a Morse function. The configuration space $\mathcal{M}$ is then the one-dimensional space of $x (\equiv n/N)$. The sub-manifold $\mathcal{M}_v$ defined by

$$\mathcal{M}_v = \{ x \in \mathcal{M} | \; \bar{p}(x) \simeq \exp(-NV_0(x)) \leq v \} \quad , \tag{45}$$

then describes the change of topology close to the second-order phase transitions θ_0^*. This will be true for all second-order transitions discussed below. We observe that for finite N the change in topology, i.e. the appearance of an additional disjoint x-interval due to the appearance of a new local maximum in $\bar{p}(x)$, in general occurs before the actual second-order phase transition.

Critical points where new extrema of $V_0(x)$ appear are determined by $V_0''(x) = 0$, i.e. non-trivial solutions of

$$\tan \phi = \phi \quad , \tag{46}$$

independent of the physical parameters of the micromaser. This equation has infinitely many positive solutions $\phi = \phi_k$, where $k = 1, 2, \dots$. Corresponding to these solutions we have the critical pump parameters $\theta_k \equiv \theta(\phi_k)$, i.e

$$\theta_k = \frac{1}{\sqrt{2a - 1}} \frac{\phi_k}{|\sin \phi_k|} \quad , \quad k = 1, 2, 3, \dots \quad , \tag{47}$$

independent of n_b and Δ, for which the k'th branch comes into existence. For a given branch $k \geq 1$, the $V_0''(x(\phi)) > 0$ sub-branches and the $V_0''(x(\phi)) < 0$ sub-branch coin-
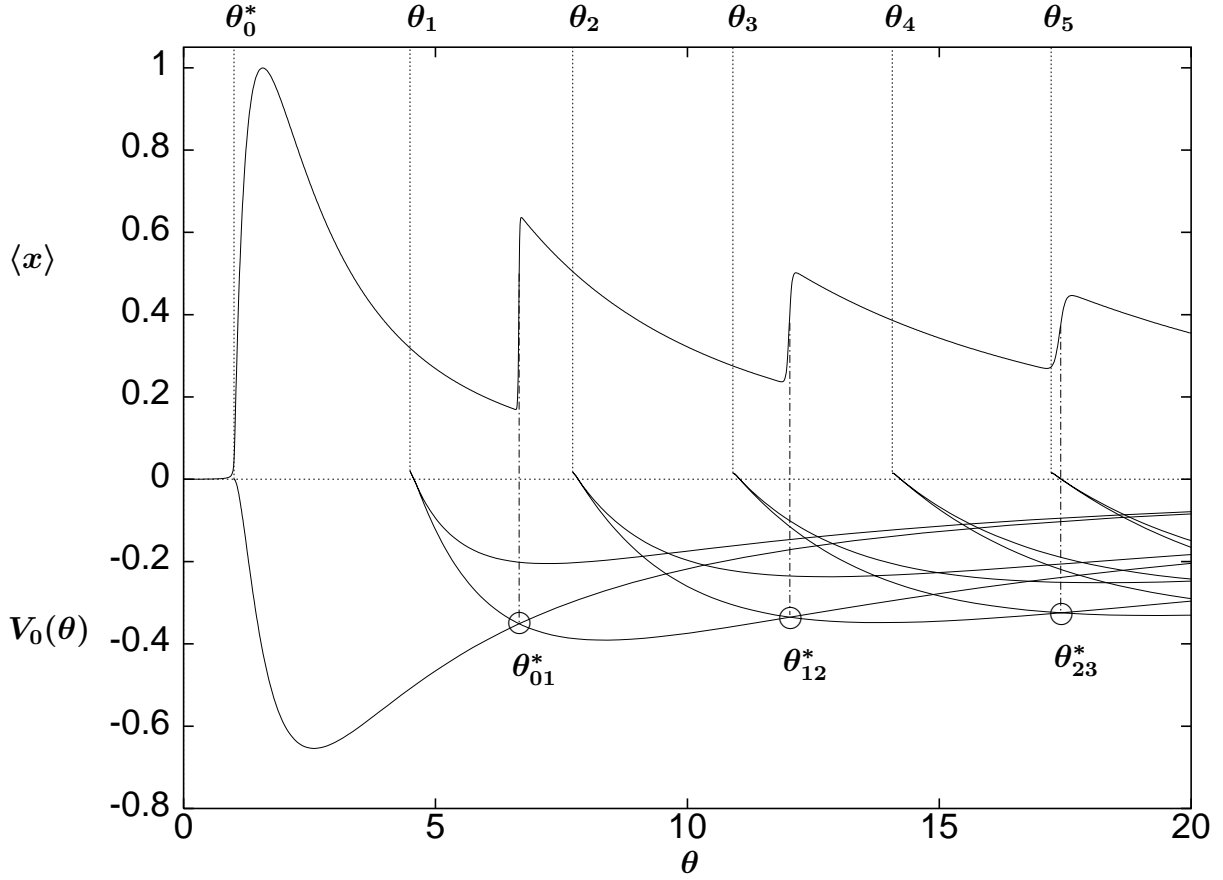
Figure 1: The order parameter $\langle x \rangle = \langle n \rangle / N$, as a function of θ, when $a = 1$, $\Delta = 0$, $n_b = 0.15$ and $N = 1000$. A dotted vertical line at $\theta = \theta_k$, where $\theta_0 = \theta_0^*$, indicates where the k:th branch comes into existence. θ_0^* corresponds to a second-order phase transition. The numerical values of the pump parameters are: $\theta_0^* = 1$, $\theta_1 = 4.603$, $\theta_2 = 7.790$, $\theta_3 = 10.950$, $\theta_4 = 14.102$ and $\theta_5 = 17.250$. The various branches at the extremum of the effective potential, i.e. $V_0(\theta) = V_0(\phi, \theta(\phi))$, are also shown. The intersection between two neighbouring $V_0''(x(\phi)) > 0$ sub-branches at $\theta = \theta_{kk+1}^*$ is marked by a circle when this coincidence occurs at a global minimum of $V_0(\theta)$. At these first-order maser-to-maser phase transitions the order parameter $\langle x \rangle$ makes a discontinuous change in the large N limit. The numerical values of the transition parameters θ_{kk+1}^* are: $\theta_{01}^* \approx 6.6610$, $\theta_{12}^* \approx 12.035$ and $\theta_{23}^* \approx 17.413$.

12
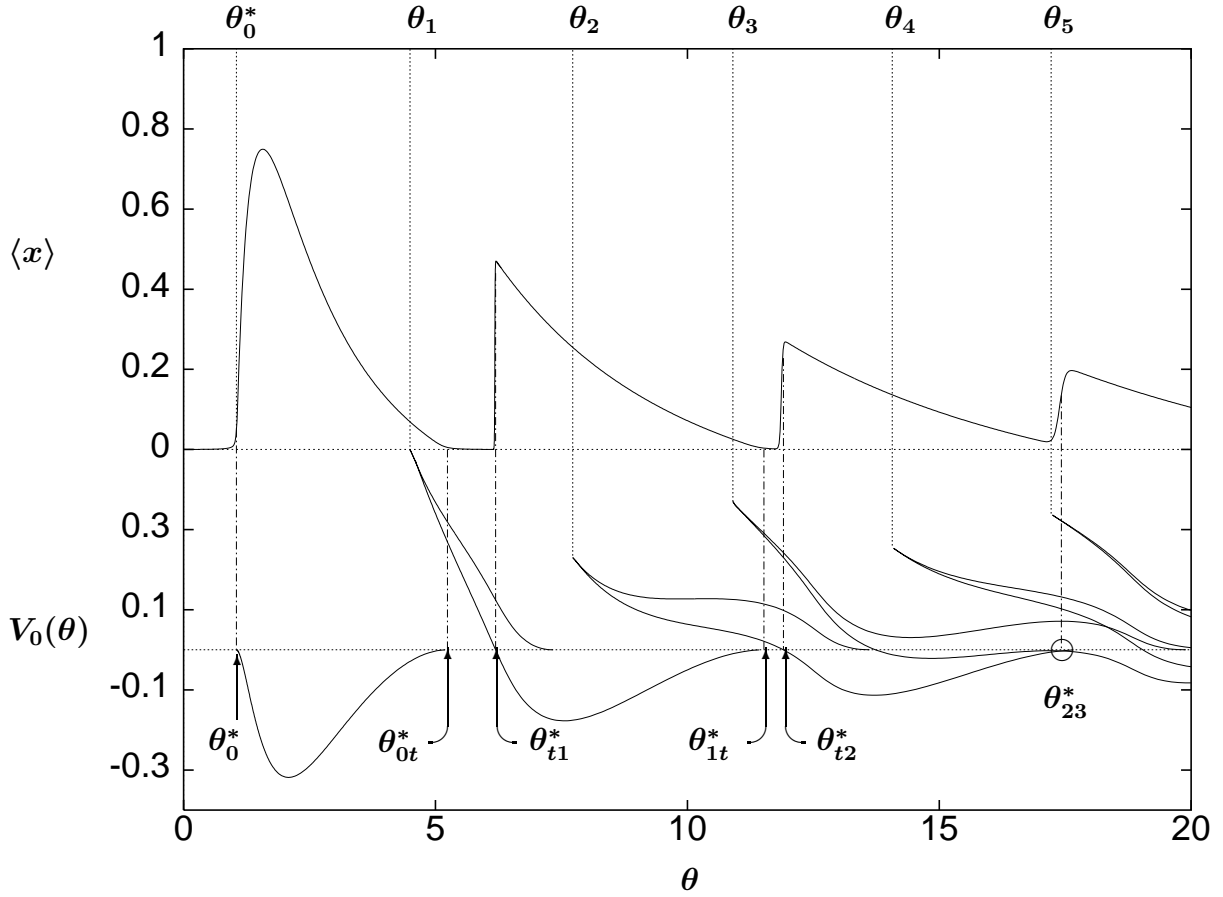
Figure 2: The order parameter $\langle x \rangle = \langle n \rangle / N$, as a function of θ, when $|\Delta| = 0.5$ and all other parameters as in Fig. 1. A dotted vertical line at $\theta = \theta_k$, where $\theta_0 = \theta_0^*$, indicates where the k:th branch comes into existence. The numerical value of θ_0^* is $\theta_0^* = 1.047$. The numerical value of the θ_k, $k \neq 0$, is the same as in Fig. 1 since this critical θ only depends on a. The various branches at the extremum of the effective potential, i.e. $V_0(\theta) = V_0(\phi, \theta(\phi))$, are also shown. First-order thermal-to-maser phase transitions occur at the pump parameters θ_{tk}^* and second-order maser-to-thermal transitions occur at θ_0^*, θ_{0t}^* and θ_{kt}^*. The circle at $\theta = \theta_{23}^*$ in the figure indicates a maser-to-maser transition. The numerical values of the critical transition parameters in the figure are: $\theta_0^* \approx 1.047$, $\theta_{0t}^* \approx 5.236$, $\theta_{t1}^* \approx 6.193$ $\theta_{1t}^* \approx 11.519$, $\theta_{t2}^* \approx 11.906$ and $\theta_{23}^* \approx 17.425$.

13

cide at this particular critical point θ_k (see e.g. Fig. 1). The critical point $\theta = \theta_k$ also corresponds to $x'(\theta_k) = \infty$ as seen from Eq. (44).

Each sub-branch with $V_0''(x(\phi)) > 0$ of the effective potential $V_0(\theta)$ has one and only one minimum. This can be seen from the expression

$$\frac{d V_0(\theta)}{d\theta} = -\frac{2}{\theta(\phi)}[a + n_b(2a - 1)] \, J(\phi) \quad , \tag{48}$$

where

$$J(\phi) \equiv \int_{\phi_0 + k\pi}^{\phi} d\chi \, \chi^4 \frac{\sin(2\chi)}{\left[\chi^2 n_b + a \, \theta(\phi)^2 \sin^2 \chi\right] \left[\chi^2(1 + n_b) + b \, \theta(\phi)^2 \sin^2 \chi\right]} \quad , \tag{49}$$

and $V_0(\theta) = V_0(\phi, \theta(\phi))$. The upper integration limit ϕ must then be chosen according to Eq. (29) where we, of course, only consider the $V_0''(x(\phi)) > 0$ sub-branch for $k \geq 1$.

We can now study the actual intersections of the various branches at a common global minimum by making use of numerical and analytical methods. The procedure is, for example, illustrated in Fig. 1 and Fig. 2. We find that $V_0(\theta)$ is such that if two branches do intersect at a common global minimum, these branches correspond to k and $k + 1$, i.e. they are consecutive branches. A given branch can also intersect with $V_0(\theta) = 0$, i.e. the thermal phase. In addition two consecutive branches can intersect when $V_0(\theta) = 0$. We then have a triple point.

3.2 The Critical Parameters θ_{kk+1}^*, θ_{tk}^* and θ_{kt}^*

If, for a given a, n_b and Δ, we have a transition from the maser branch k to the neighbouring maser branch $k + 1$, then there exist a ϕ_k^* and ϕ_{k+1}^* such that

$$V_0(\phi_k^*) = V_0(\phi_{k+1}^*) \quad \text{and} \quad \theta(\phi_k^*) = \theta(\phi_{k+1}^*) \equiv \theta_{kk+1}^* \quad , \tag{50}$$

where

$$V_0(\phi_k^*) = -\frac{2}{\theta(\phi_k^*)^2} \int_{\theta(\phi_k^*)|\Delta|}^{\phi_k^*} d\phi \, \phi \, \ln[\, w(\phi, \theta(\phi_k^*))\,] \quad , \tag{51}$$

and where ϕ_k^* is in the interval $\phi_k < \phi_k^* < (\pi - \phi_0) + k\pi$. The reason why we chose $\phi_k^* > \phi_k$ is that we are looking for solutions of Eq. (51) for which $V_0''(x(\phi)) > 0$. The pump parameter according to Eq. (50) can be expressed as

14

$$\theta_{k k+1}^* = \frac{1}{\sqrt{2a-1}} \frac{\phi_k^*}{|\sin \phi_k^*|} \quad . \tag{52}$$

Furthermore, for this particular combination of the parameters, the order parameter $\langle x \rangle = \langle n \rangle / N$ makes a discontinous change as can be seen from the Eq. (26), i.e. the discontinuity in $\langle x \rangle$ is given $\Delta \langle x \rangle = x(\phi_{k+1}^*) - x(\phi_k^*)$. We therefore have a first-order phase transition.

If, on the other hand, a given maser branch corresponding to a global minima does not intersect with a neighbouring maser branch, it is the intersection with the thermal branch which determines the phase transition (see e.g. Fig. 2). For a given branch $k \geq 1$, let $\theta_{tk}^* \equiv \theta(\phi_{tk}^*)$ denote the pump parameter of this thermal-to-maser transition. The value of ϕ_{tk}^* is then determined by the solution of

$$V_0(\phi_{tk}^*) = 0 \quad , \tag{53}$$

where

$$V_0(\phi_{tk}^*) = -\frac{2}{\theta(\phi_{tk}^*)^2} \int_{\theta(\phi_{tk}^*)|\Delta|}^{\phi_{tk}^*} d\phi \, \phi \, \ln[\, w(\phi, \theta(\phi_{tk}^*))\,] \quad . \tag{54}$$

We determine ϕ_{tk}^* numerically, where $\phi_k < \phi_{tk}^* < (\pi - \phi_0) + k\pi$ and $k = 1, 2, 3, \dots$. The corresponding pump parameters are $\theta_{tk}^* \equiv \theta(\phi_{tk}^*)$, i.e

$$\theta_{tk}^* = \frac{1}{\sqrt{2a-1}} \frac{\phi_{tk}^*}{|\sin \phi_{tk}^*|} \quad , \quad k = 1, 2, 3, \dots \quad . \tag{55}$$

Due to the same reasons as discussed above, such thermal-to-maser transitions correspond to first-order phase transitions.

Furthermore, let $\theta_{kt}^* \equiv \theta(\phi_{kt}^*)$ denote the maser-to-thermal transition for a given branch $k \geq 0$ (see e.g. Fig. 2). The value of ϕ_{kt}^* is determined by one of the solutions of
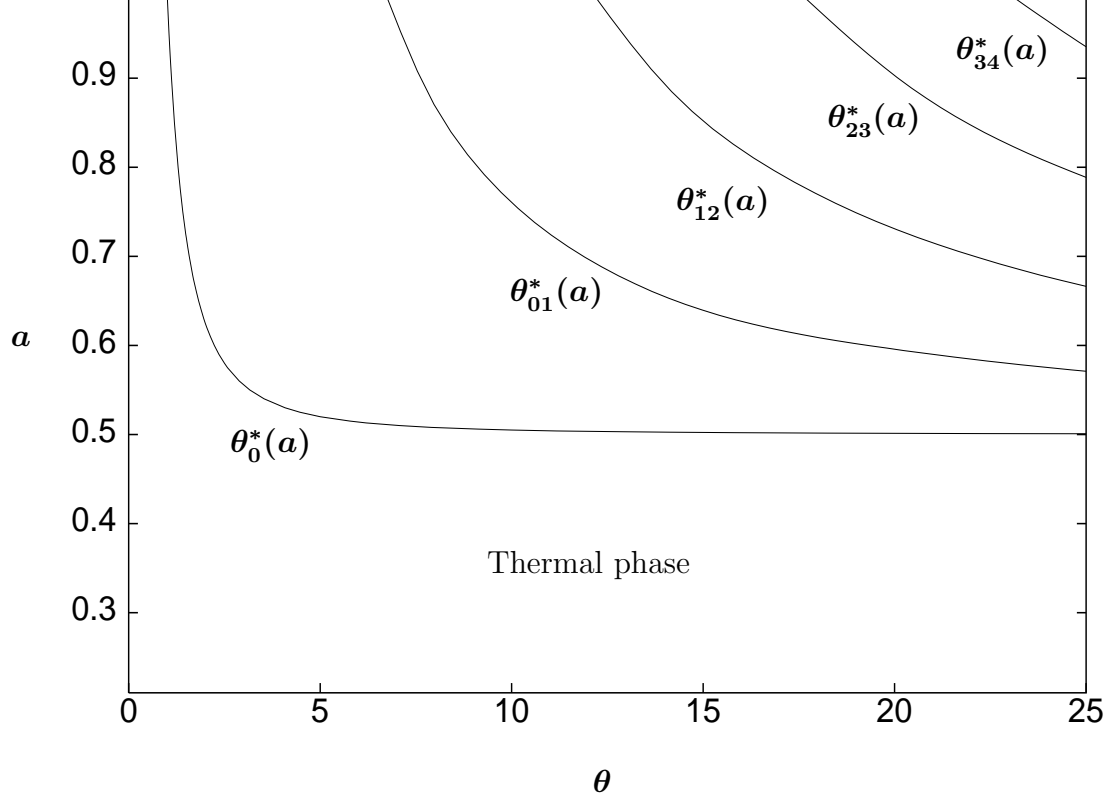
$$V_0(\phi_{kt}^*) = 0 \quad , \tag{56}$$

where

$$V_0(\phi_{kt}^*) = -\frac{2}{\theta(\phi_{kt}^*)^2} \int_{\theta(\phi_{kt}^*)|\Delta|}^{\phi_{kt}^*} d\phi \, \phi \, \ln[\, w(\phi, \theta(\phi_{kt}^*))\,] \quad . \tag{57}$$

We see that

$$\phi_{kt}^* = (\pi - \phi_0) + k\pi \quad , \tag{58}$$

Figure 3: The phase diagram for the micromaser system when $n_b = 0.15$ and $\Delta = 0$. All the critical lines converge to $1/2$ in the large θ limit. The thermal-to-maser critical line $\theta_0^*(a)$ is determined analytically by Eq. (43). The other critical lines $\theta_{kk+1}^*(a)$, which are maser-to-maser transitions, are determined by Eq. (52).

for all branches $k \geq 0$. When $\Delta \neq 0$, Eq. (56) is trivially fulfilled since the upper integration limit is equal to the lower. If, on the other hand, $\Delta = 0$, then Eq. (56) is fulfilled since $\theta(\phi_{kt}^*) = \infty$. The pump parameter $\theta_{kt}^* \equiv \theta(\phi_{kt})$ is given by

$$\theta_{kt}^* = \frac{(k+1)\pi - \arcsin(|\Delta|/\sqrt{2a-1})}{|\Delta|} \quad , \quad k = 0, 1, 2, \ldots \quad . \tag{59}$$

This equation is equivalent to

$$a = \frac{1}{2} + \frac{\Delta^2}{2\sin^2(\theta_{kt}^*\Delta)} \quad , \quad k = 0, 1, 2, \ldots \quad , \tag{60}$$

which is of the same form as Eq. (42). Due to the same reasons as discussed above, such a maser-to-thermal transition corresponds to a second-order phase transition.

Equipped with these results, we can now construct a complete phase diagram in e.g. the a- and θ-parameter space for a given n_b and Δ.

16

3.3 Phase Diagram

The phase diagram when $n_b = 0.15$ and $\Delta = 0$ is shown in Fig. 3. The first critical line in this figure is given by Eq. (43). As already mentioned, this corresponds to a second-order thermal-to-maser phase transition. In the region above this line the mean occupation number $\langle n \rangle$ grows proportionally with the pumping rate N. The cavity therefore behaves like a maser in this regime. For values of a and θ below this line the only global minimum of $V_0(x)$ occurs at $x = 0$. In this particular region the probability $\bar{p}_n$ is given by the thermal distribution in Eq. (21), i.e. the micromaser is in the thermal phase. We remark too that Eq. (42) also determines the radius of converegence of the thermal probability distribution in Eq. (21). The other critical lines in Fig. 3 are determined by Eq. (50) since for $n_b = 0.15$ and $\Delta = 0$, all neighbouring $V_0''(x(\phi)) > 0$ sub-branches of $V_0(\theta) = V_0(\phi(\theta), \theta)$ intersect for some $a > 1/2$, see Fig. 1.

When the micromaser is detuned the phase diagram is more complicated. Fig. 4 shows a typical example of a phase diagram when $\Delta \neq 0$. As we can see from this figure, the first two maser phases are well separated. The critical value of Δ for such a separation of phases is in general determined by considering phase separation on the line $a = 1$. For a given n_b, let $\Delta = \Delta_{kk+1}$ be the corresponding critical value for phase separation. With the definition $\phi_{t0}^* \equiv \phi_0$, where ϕ_0 is given in Eq. (28), Δ_{kk+1} is determined by the transcendental equation

$$\theta(\phi_{kt}^*) = \theta(\phi_{tk}^*) \quad , \quad k = 0, 1, 2, \dots \quad , \tag{61}$$

i.e. the solution of

$$|\Delta| = \frac{|\sin \phi_{tk}^*|}{\phi_{tk}^*} \left[(k+1)\pi - \arcsin |\Delta| \right] \quad . \tag{62}$$

Here ϕ_{tk}^* is determined numerically according to Eq. (53). For $n_b = 0.15$ the first critical value of detuning is $|\Delta_{01}| \approx 0.408$. When the detuning is larger than Δ_{kk+1}, branch k will separate from branch $k+1$ (see e.g. Fig. 4). In passing, we notice that Δ_{kk+1} is restricted by $\Delta_{kk+1}^2 < 1$, for all possible branches.

The first critical line in Fig. 4 corresponds to a second-order thermal-to-maser (maser-to-thermal) transition to the left (right) of its minimum. The minima of the critical lines are marked by short vertical lines. For any other critical line in Fig. 4 the transition is a first-order thermal-to-maser (second-order maser-to-thermal) phase transition to the left (right) of its minimum unless it intersects with another critical line. In the region between

17
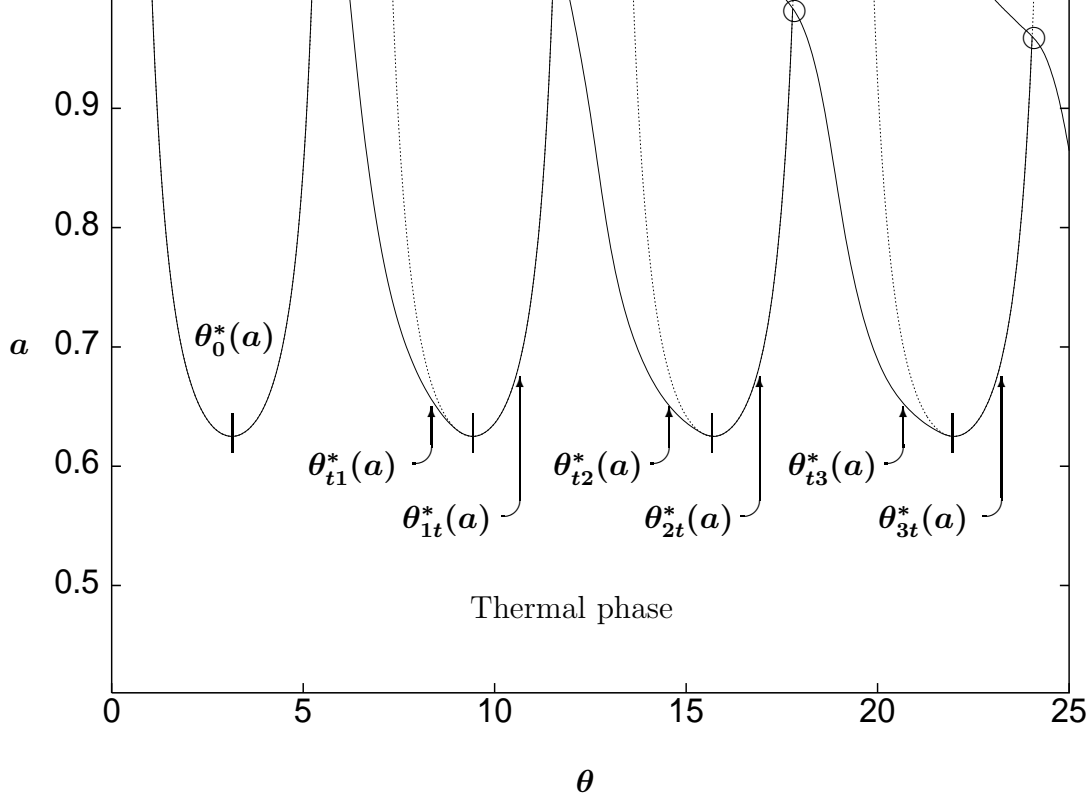
Figure 4: The phase diagram for the micromaser system when $n_b = 0.15$ and $|\Delta| = 0.5$. In this diagram we have plotted the range of validity of the thermal distribution (dotted lines). When not visible these dotted lines overlap with the solid critical lines. The minima of the critical lines are determined by the condition $\sin^2(\Delta\theta) = 1$ and are marked by a short vertical lines. The first critical line $\theta_0^*(a)$ in this phase diagram is determined analytically by Eq. (41). The critical lines $\theta_{tk}^*(a)$ are given by Eq. (55) and $\theta_{kt}^*(a)$ are given by Eq. (59). Triple points are indicated by circles. The numerical values of these triple points are $(a_{23}, \theta_{23})^{triple} = (0.98, 17.78)$ and $(a_{34}, \theta_{34})^{triple} = (0.96, 24.04)$.

any thermal-to-maser line and the neighbouring dotted line, the thermal probability distribution does not correspond to a global minimum of $V_0(x)$. The phase diagram in Fig. 4 also contains triple points. These points are marked by circles. They are mathematically determined by

$$V_0(\phi_{tk}^*) = V_0(\phi_{kt}^*) = 0 \text{ and } \theta(\phi_{tk}^*) = \theta(\phi_{kt}^*) . \tag{63}$$

18

4   THE ORDER PARAMETER

When the system is in a maser phase the probability distribution is given by Eq. (33). $\langle x \rangle = \langle n \rangle / N$ is then, of course, trivial to compute. For a given a, Δ and θ $\langle x \rangle$ is simply given by

$$\langle x \rangle = x_j \quad , \tag{64}$$

where x_j is the value of x where $V_0(x)$ reaches its global minimum, i.e. x_j is one of the saddle-points as determined by Eq. (24). In the maser regime, the photon number behaviour (see e.g. Fig. 1) is well-established in the literature (see e.g. Refs.[1]).

For values of a and θ corresponding to the first critical line Eq. (41), the order parameter $\langle x \rangle$ is zero. Mathematically this follows trivially by substituting ϕ_0 in Eq. (28) into Eq. (26) and using Eq. (64). Below this critical line, the micromaser is in the thermal phase and the order parameter is then given by

$$\langle x \rangle = \frac{1}{N} \frac{n_b + a\,\theta_{eff}^2}{1 + (1 - 2a)\,\theta_{eff}^2} \quad , \tag{65}$$

which is zero in the large N limit. We realize from Eq. (65) that the photon number $\langle n \rangle$ is in general a periodic function of θ when the system is detuned. The period of $\langle n \rangle$ is then $|\Delta|\theta$. It reaches its maximum $(n_b + a/\Delta^2)/(1 + (1 - 2a)/\Delta^2)$ for $\Delta\theta = (n + 1/2)\pi$, where $n = 0, 1, \dots$. The minimum of $\langle n \rangle$ is n_b and occurs for $|\Delta|\theta = n\pi$. In passing, we note that the maximum value $(n_b + a/\Delta^2)/(1 + (1 - 2a)/\Delta^2)$ is reduced to n_b in thermal equilibrium, for any n_b, Δ and θ. We also note that when $n_b = 0$ the cavity is dark, i.e. $\langle x \rangle = 0$ for every integer multiple of $\theta = \pi/|\Delta|$.

When the system is not detuned, Eq. (65) is not oscillating and it then reduces to

$$\langle n \rangle = \frac{n_b + a\,\theta^2}{1 + (1 - 2a)\,\theta^2} \quad . \tag{66}$$

In the large θ limit, Eq. (66) converges to $a/(1 - 2a)$ (see Fig. 5).

The order parameter $\langle x \rangle$ can also be studied as a function of the probability a for the pump atoms to be in an excited state. Varying a over all allowed values keeping other physical parameters fixed, the order parameter $\langle x \rangle$ makes a discontinuous change for every combination of the physical parameters corresponding to a critical line. Hence, $\langle x \rangle$ as a function of a exhibits a plateau-like behaviour when N is sufficiently large. Such
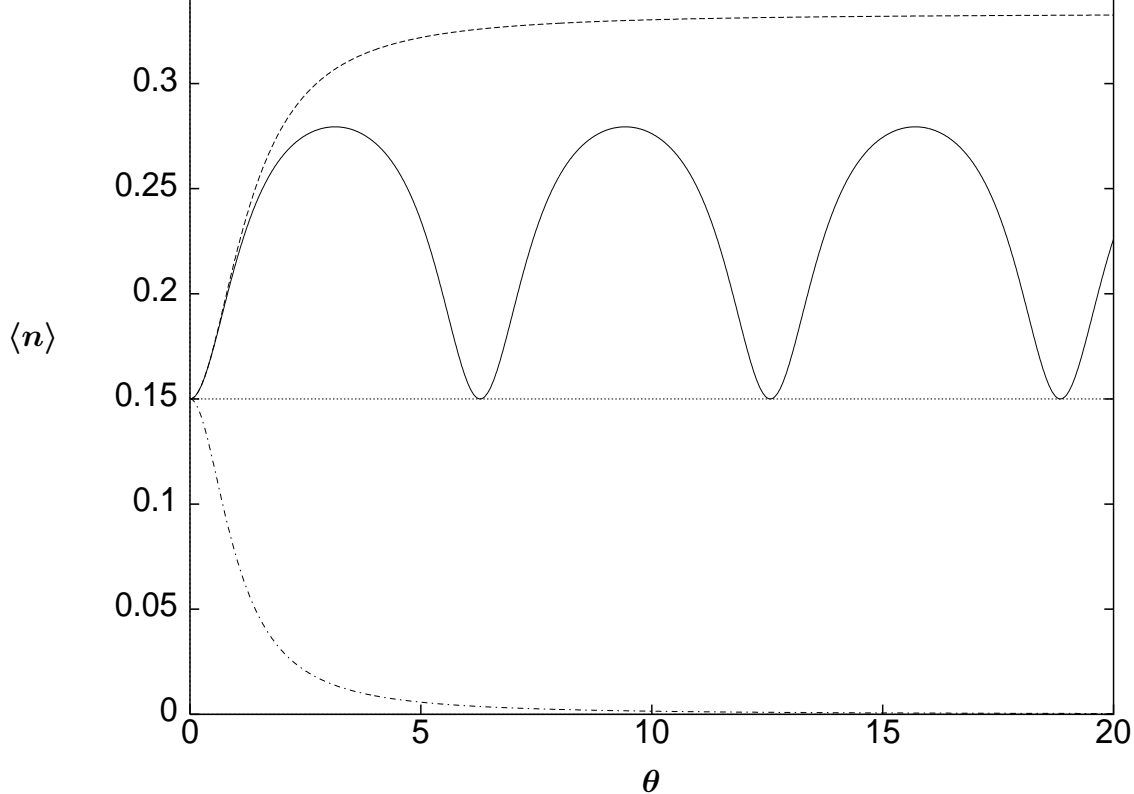
Figure 5: This figure shows the different behaviours of Eq. (65). $n_b = 0.15$ for all curves. The straight line corresponds to $a = n_b/(1 + 2\,n_b) = 3/26$, i.e. thermal equilibrium. The solid curve corresponds to $a = 0.2$ and $|\Delta| = 0.5$. The fat dotted curve corresponds to $a = 0.2$ and $\Delta = 0$. The dashed-dotted curve corresponds to $a = 0$ and $\Delta = 0$.

a behaviour is illustrated in Fig. 6. In this figure we observe a rather slow N convergence to this plateau-like behaviour.

4.1   Twinkling and Detuning

Above we have observed that the mean value $\langle n \rangle$ may oscillate as a function of θ when the micromaser is in the thermal phase. We say that the system is then in a twinkling mode. This twinkling behaviour has a close resemblance to the observed atomic inversion revivals [21, 22].

A somewhat different twinkling behaviour of the micromaser system occurs when the thermal phase intersects with a maser phase. This feature is illustrated in Fig. 4 with $|\Delta| = 0.5$ and $n_b = 0.15$. For a given $a > 1/2 + \Delta^2/2$ we then see that the system has repeated thermal-to-maser and maser-to-thermal transitions as θ increases. This twinkling behaviour is not strictly periodic in θ. The winkling phenomena will now, however, be
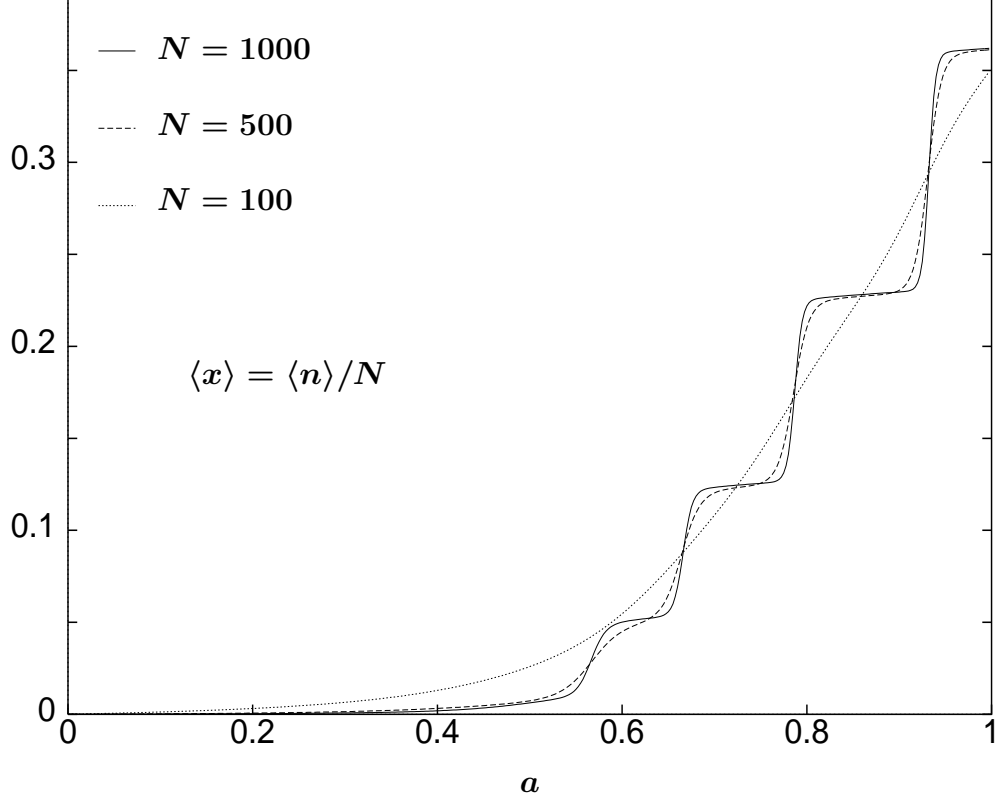
Figure 6: The order parameter $\langle x \rangle = \langle n \rangle / N$ as a function of a when $n_b = 0.15$, $\Delta = 0$, $\theta = 25$ and $N = 100, 500, 1000$. Each step in $\langle x \rangle$ corresponds to a point on one of the transition curves in Fig. 3.

more pronounced since, for large N, the maser will be "dark" in the thermal phase, but $\langle n \rangle$ is large in the maser phase since $\langle n \rangle$ is proportional to N in this region.

5 THE CORRELATION LENGTH

In this section we study long-time correlations in the large N limit. This notion of a correlation length for the micromaser system was first introduced in Refs. [9]. These correlations have a surprisingly rich structure and reflect global properties of the stationary photon distribution. The probability $\mathcal{P}(s)$ of finding an atom in a state $s = \pm$ after the interaction with the cavity, where $+$ represents the excited state and $-$ represents the ground state, can be expressed in the following matrix form [9]:

$$\mathcal{P}(s) = \bar{u}^{0^T} M(s) \bar{p} \quad , \tag{67}$$

such that $\mathcal{P}(+) + \mathcal{P}(-) = 1$. The elements of the vector $\bar{p}$ are given the equilibrium

distribution in Eq. (8), and the matrix $M(s)$ is given by Eqs.(5) and (6). The quantity $\bar{u}^0$ is a vector with all entries equal to 1, $\bar{u}_n^0 = 1$. Furthermore, the joint probability for observing two atoms in the states s_1 and s_2 with a time-delay t between them, is given by [9]

$$
\begin{aligned}
\mathcal{P}(s_1, s_2, t) &= \bar{u}^{0^T} S(s_2) \, e^{-\gamma L t} \, S(s_1) \, \bar{p} \\
&= \bar{u}^{0^T} M(s_2) \, e^{-\gamma L t} \, S(s_1) \, \bar{p} \ ,
\end{aligned}
\tag{68}
$$

where L is given by Eq. (3) and where

$$
S(s) = (1 + L_C/N)^{-1} M(s) \ .
\tag{69}
$$

We observe that $\mathcal{P}(+, -, t) = \mathcal{P}(-, +, t)$ [9], which means that the cavity photons and the outgoing atoms are not quantum-mechanically entangled. Statistical correlations do, however, exist.

A properly normalised correlation function is then defined by

$$
\gamma^A(t) = \frac{\langle ss \rangle_t - \langle s \rangle^2}{1 - \langle s \rangle^2} \ ,
\tag{70}
$$

where $\langle ss \rangle_t = \sum_{s_1, s_2} s_1 s_2 \mathcal{P}(s_1, s_2, t)$ and $\langle s \rangle = \sum_s s \, \mathcal{P}(s)$. This correlation function satisfies $-1 \le \gamma^A(t) \le 1$. At large times $t \to \infty$, we then define the atomic beam correlation length ξ_A by [9]

$$
\gamma_A(t) \simeq e^{-t/\xi_A} \ .
\tag{71}
$$

The lowest eigenvalue $\lambda = 0$ of L determines the stationary equilibrium solution $\bar{p}$. The next non-zero eigenvalue λ_{nz} of L, on the other hand, determines the typical time scales for the approach to the stationary situation. This eigenvalue can be determined numerically. The relation between λ_{nz} and the atomic beam correlation length is $1/\xi_A = \gamma \lambda_{nz}$. For photons we define a similar correlation length ξ_C. It follows that the correlation lengths are identical, i.e. $\xi_A = \xi_C \equiv \xi$ [9].

The correlation length $\gamma \xi$ is shown in Fig. 7 ($\Delta = 0$) and Fig. 8 ($|\Delta| = 0.5$) for various values of N. Furthermore, Fig. 9 shows $\gamma \xi$ for various values of the detuning. When the detuning is sufficiently small, we observe from these figures that the correlation length exhibits large peaks for different values of θ. In the large N limit, numerical studies reveal that these large peaks occur at the transition parameters θ_0^*, θ_{kk+1}^* and/or θ_{tk}^*, depending
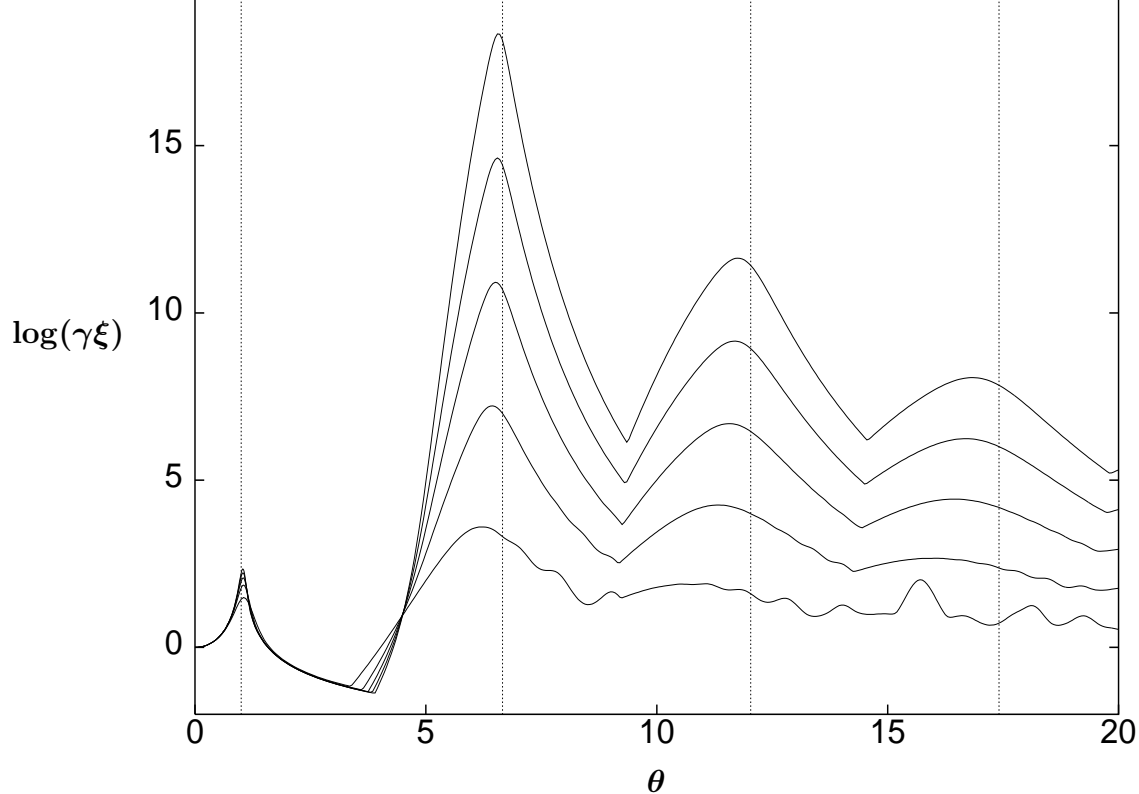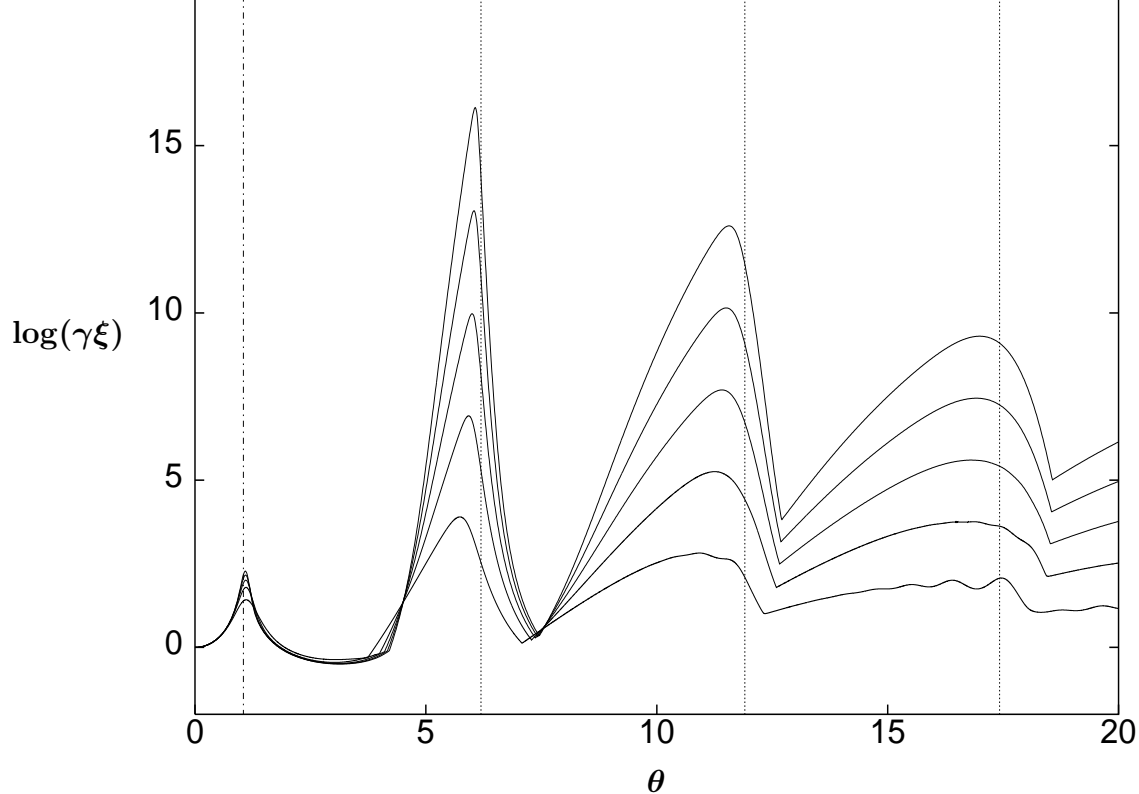
Figure 7: The logarithm of the correlation length $\gamma\xi$ as a function of θ for various values of $N = 25, 50, ..., 125$ when $n_b = 0.15$, $\Delta = 0$ and $a = 1$. The numerical values of the vertical lines are as in Fig. 1.

on the values of the given n_b and Δ (see e.g. Fig. 7 and Fig. 8). We will discuss the behaviour of these peaks in more detail in Section 5.4. When the detuning is sufficiently large, i.e. $\Delta^2 > 2a - 1$, the correlation becomes smaller and behaves in a strictly periodic manner as a function of the pump parameter θ (see e.g. Fig. 9).

In order to arrive at a better understanding of the behaviour of the correlation length, we will derive various approximative expressions in the following subsections. We will use three different methods in order to derive such expressions for ξ and we will compare them with the exact numerical results.

5.1 The Eigenvalue Value Method

By making use of the orthonormality conditions for the left (u_n) and right (p_n) eigenvectors corresponding to the eigenvalue problem as defined by Eq. (2), i.e. $u^T L = \lambda u^T$ and $Lp = \lambda p$, it is shown in [9] that an eigenvalue satifies the equation

Figure 8: The logarithm of the correlation length $\gamma\xi$ as a function of θ for various values of $N = 25, 50, ..., 125$ when $n_b = 0.15$, $|\Delta| = 0.5$ and $a = 1$. The numerical values of the vertical lines are as in Fig. 2.

$$\lambda = \sum_{n=0}^{\infty} p_n B_n (u_n - u_{n-1})^2 \quad , \tag{72}$$

where

$$B_n = (n_b + 1)n + Nbq_n \quad . \tag{73}$$

and $p_n = \bar{p}_n^0 u_n$. The left eigenfunction u_n corresponding to the first non-zero eigenvalue λ_{nz} has one node. It is natural to assume that this node occurs at $\langle n \rangle$. This is so since in the neighbourhood of $\langle n \rangle$ we can then use the Ansatz

$$u_n = \frac{n - \langle n \rangle}{\sigma_n} \quad , \tag{74}$$

where $\sigma_n^2 = \langle n^2 \rangle - \langle n \rangle^2$ as usual. The average values are assumed to be taken over the equilibrium distribution $\bar{p}_n$. It then follows that $u \cdot \bar{p} = \langle u_n \rangle = 0$ and $u \cdot p = \langle u_n^2 \rangle = 1$. By the Ansatz Eq.(74) it now follows that

$$\gamma\xi \simeq \gamma\xi_E(\theta) = \frac{\sigma_n^2}{(n_b + 1)\langle n \rangle + Nb \langle q_n \rangle} \quad , \tag{75}$$

24
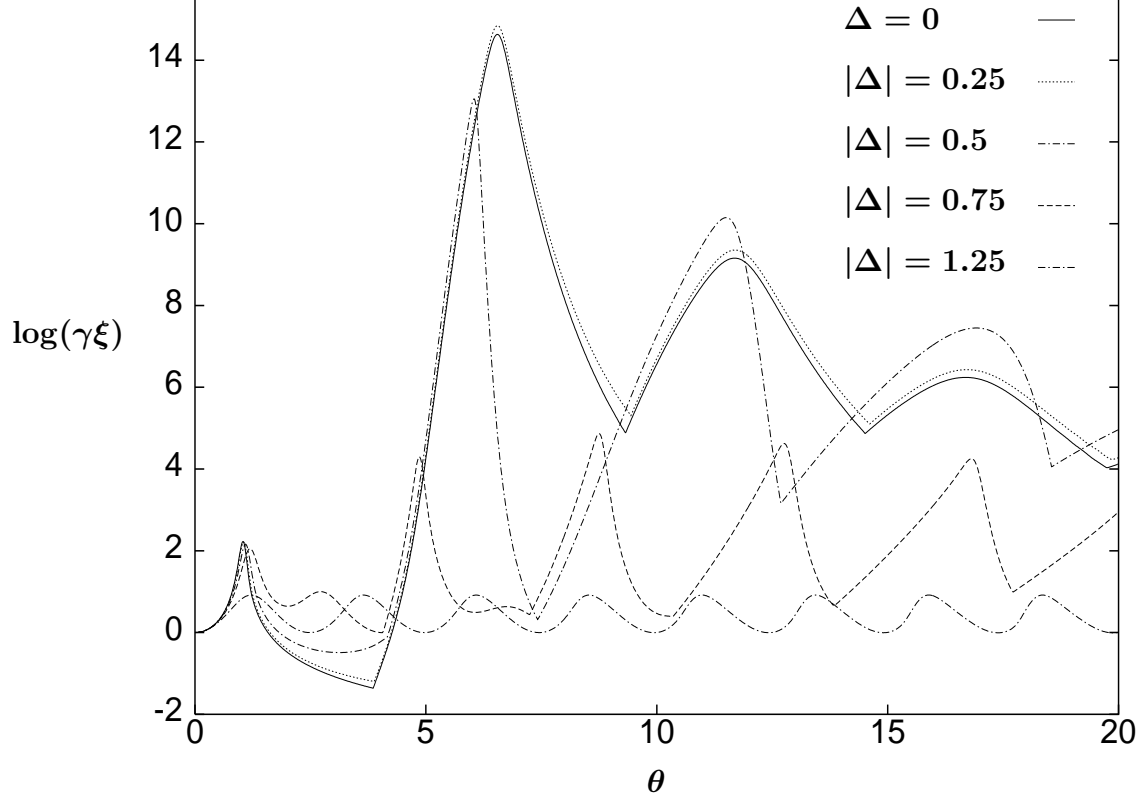
Figure 9:   The logarithm of the correlation length $\gamma\xi$ as a function of θ for various values of $|\Delta| = 0$, 0.25, 0.50, 0.75 and 1.25 when $n_b = 0.15$, $a = 1$ and $N = 100$.

since $\gamma\xi = 1/\lambda_{nz}$. Eq. (75) can be simplified in the large N limit. In this case we have $\langle q_n \rangle \approx \theta_{eff}^2 \langle n \rangle / N$. If, in addition, the micromaser is in the thermal phase, then Eq. (75) reduces to

$$\gamma\xi_E(\theta) = \frac{1}{1 - (2a-1)\theta_{eff}^2} \quad , \tag{76}$$

which explains the periodic behaviour of the correlation as mentioned in the beginning of this section. We also observe that $\gamma\xi_E = 1$ when $a = 1/2$, independent of any of the other physical parameters at hand.

5.2   The Master Equation Method

Let us now derive an approximative expression for the correlation length by making use of another method. For a general right eigenvector of the matrix L we define $p(x) = Np_n$ and write it as $p(x) = \bar{p}(x)u(x)$ with the left eigenvector $u(x) = u_n$. It is then shown in [9] that

$$\lambda\,u(x) = [\,x - (2a - 1)\,q(x)\,]\,\frac{du(x)}{dx} - \frac{1}{N}\frac{d}{dx}\left[\,(\,n_b x + aq(x)\,)\frac{du(x)}{dx}\,\right] \quad, \qquad (77)$$

in the large N limit. Here we again make use of the fact that the eigenfunction corresponding to λ_{nz} has only one node, say at $x = x_0$. The function $u(x)$ is therefore given by $u(x) \approx x - x_0$ in the neighbourhood of x_0. Furthermore, when $\theta\sqrt{x(\theta) + \Delta^2} \ll 1$, we can expand $q(x)$ around $x = 0$, in which case Eq. (77) reduces to

$$\lambda_{nz}(x - x_0) = \alpha(\theta)\,x + \beta(\theta)\,x^2 - \frac{\gamma(\theta)}{N} \quad, \qquad (78)$$

where

$$\alpha(\theta) = 1 - (2a - 1)\,\theta_{eff}^2 \quad, \qquad (79)$$

$$\beta(\theta) = (2a - 1)\left[\frac{\sin^2(\theta\Delta)}{\Delta^4} - \frac{\theta\sin(\theta|\Delta|)\cos(\theta|\Delta|)}{\Delta^3}\right] \quad, \qquad (80)$$

$$\gamma(\theta) = n_b + a\,\theta_{eff}^2 \quad. \qquad (81)$$

Notice that Eq. (81) is only valid when we are not too close to a critical line. For small perturbations around x_0, i.e. $x = x_0 + \delta x$, the eigenvalue λ_{nz} is then

$$\lambda_{nz} = \alpha(\theta) + 2\beta(\theta)\,x_0 \quad, \qquad (82)$$

where x_0 is easily solved by the aid of this equation and Eq. (78):

$$x_0(\theta) = -\frac{\alpha(\theta)}{2\,\beta(\theta)} + \sqrt{\left(\frac{\alpha(\theta)}{2\,\beta(\theta)}\right)^2 + \frac{\gamma(\theta)}{\beta(\theta)\,N}} \quad. \qquad (83)$$
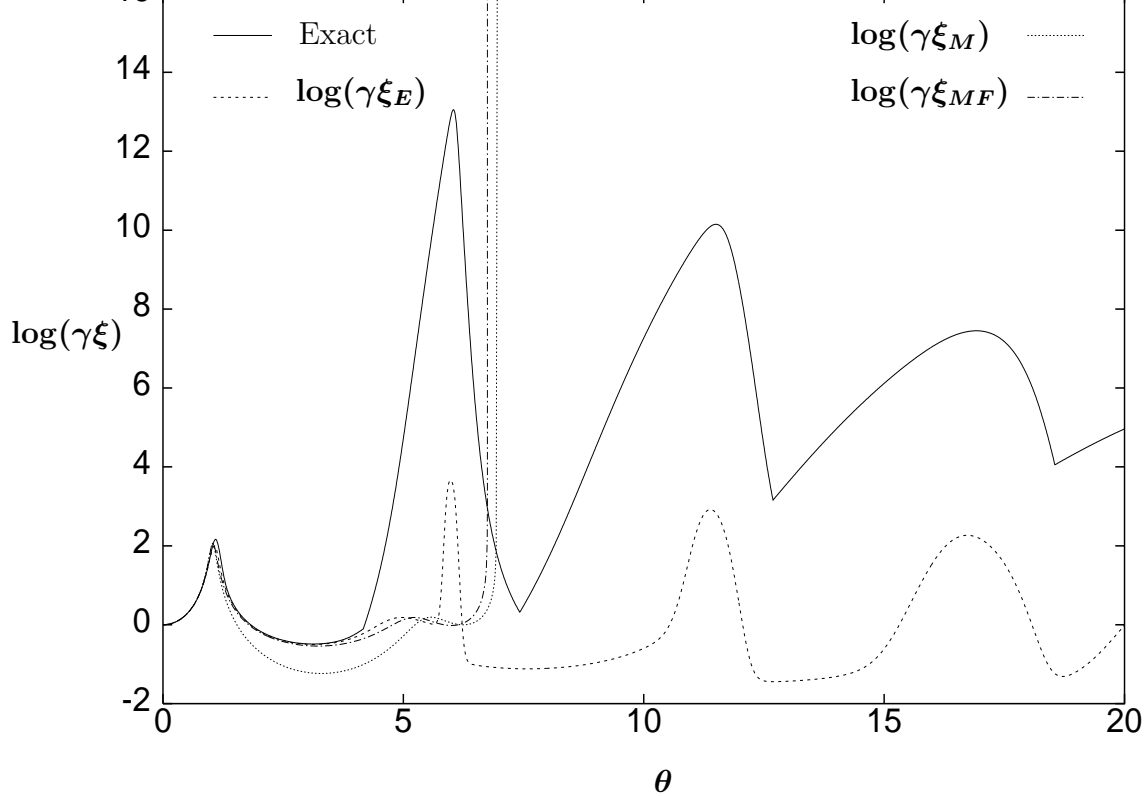
Since $1/\xi = \gamma\lambda_{nz}$, we get

$$\gamma\xi \simeq \gamma\xi_M(\theta) = \frac{1}{\sqrt{\alpha^2(\theta) + \dfrac{4\,\beta(\theta)\,\gamma(\theta)}{N}}} \quad. \qquad (84)$$

In the large N limit, where $x_0 = 0$ (see Eq. (83)), Eq. (84) is reduced to $\gamma\xi_M(\theta) = 1/\alpha(\theta)$, i.e.

$$\gamma\xi_M(\theta) = \frac{1}{1 - (2a - 1)\theta_{eff}^2} \quad, \qquad (85)$$

in agreement with Eq. (76).

Figure 10: Comparison of $\log(\gamma\xi)$ as a function of θ for various analytical expressions of the correlation. The parameters for all lines are $a = 1$, $|\Delta| = 0.5$, $n_b = 0.15$ and $N = 100$. The solid curve is the exact correlation length.

The correlation length $\xi_M(\theta)$ exhibits its first peak at $\theta = \theta_0^*$ (see e.g. Fig. 10 and Fig. 11). The correlation length Eq. (84) at this particular peak is

$$\gamma\xi_M(\theta_0^*) = \frac{2a - 1}{2} \sqrt{\frac{N}{a + n_b(2a - 1)}} \; \chi(\theta_0^*|\Delta|) \;\;, \tag{86}$$

where

$$\chi(x) = \sqrt{\frac{\sin^2 x}{1 - x \cot x}} \;\;. \tag{87}$$

In Eq. (86) the probability a can only be chosen in the interval $1/2 + \Delta^2/2 \leq a \leq 1$. This equation shows that the correlation $\theta = \theta_0^*$ grows as $\sqrt{N}$. Again we notice the factor $a + n_b(2a - 1)$. Also note that Eq. (86) vanishes when $a = 1/2$. Since by assumption $\theta|\Delta| \ll 1$, then Eq. (87) is $\chi(\theta|\Delta|) \approx \sqrt{3}\,[1 - (\theta\Delta)^2/5]$. The correlation length in Eq. (86)
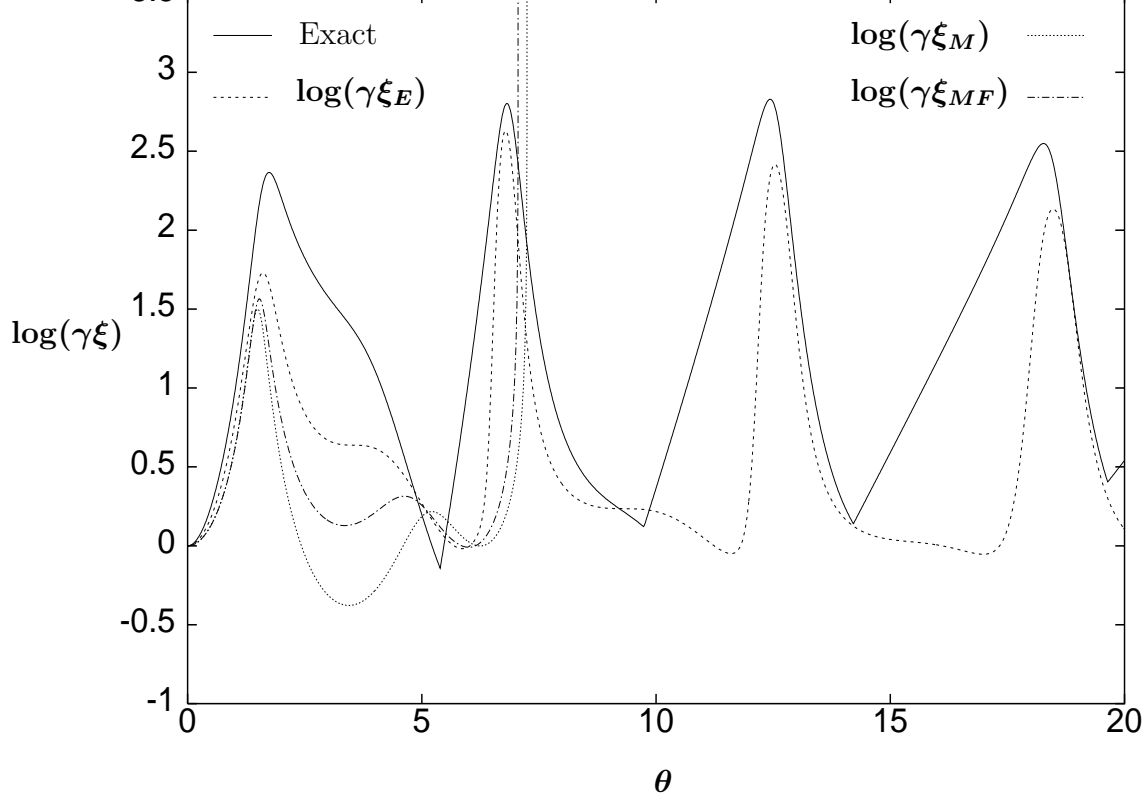
Figure 11: Comparison of $\log(\gamma\xi)$ as a function of θ for various analytical expressions derived in the text. The parameters for all curves are $a = 0.75$, $|\Delta| = 0.5$, $n_b = 0.15$ and $N = 100$. The solid curve is the exact correlation length.

is then in agreement with the results of Ref.[9] for $\Delta = 0$.

5.3 The Mean Field Approximation

We can also use a mean field approximation in order to get an approximative and analytical expression for the correlation length ξ. When the atoms have Poisson distributed arrival times, the continuous master equation gives the following exact equation for the average photon occupation number [9]:

$$\frac{1}{\gamma}\frac{d\langle x\rangle}{dt} = -\left[\langle x\rangle - \frac{n_b}{N}\right] + a\langle q_{n+1}\rangle - b\langle q_n\rangle \quad . \tag{88}$$

By making use of the mean field approximation $\langle q_n\rangle \approx q_{\langle n\rangle} = q(\langle x\rangle)$, the above equation simplifies considerably. The stationary solution, $\langle x\rangle = x_0$, of Eq. (88) is determined by a transcendent equation which, generally, can be solved numerically only. However, with the approximation
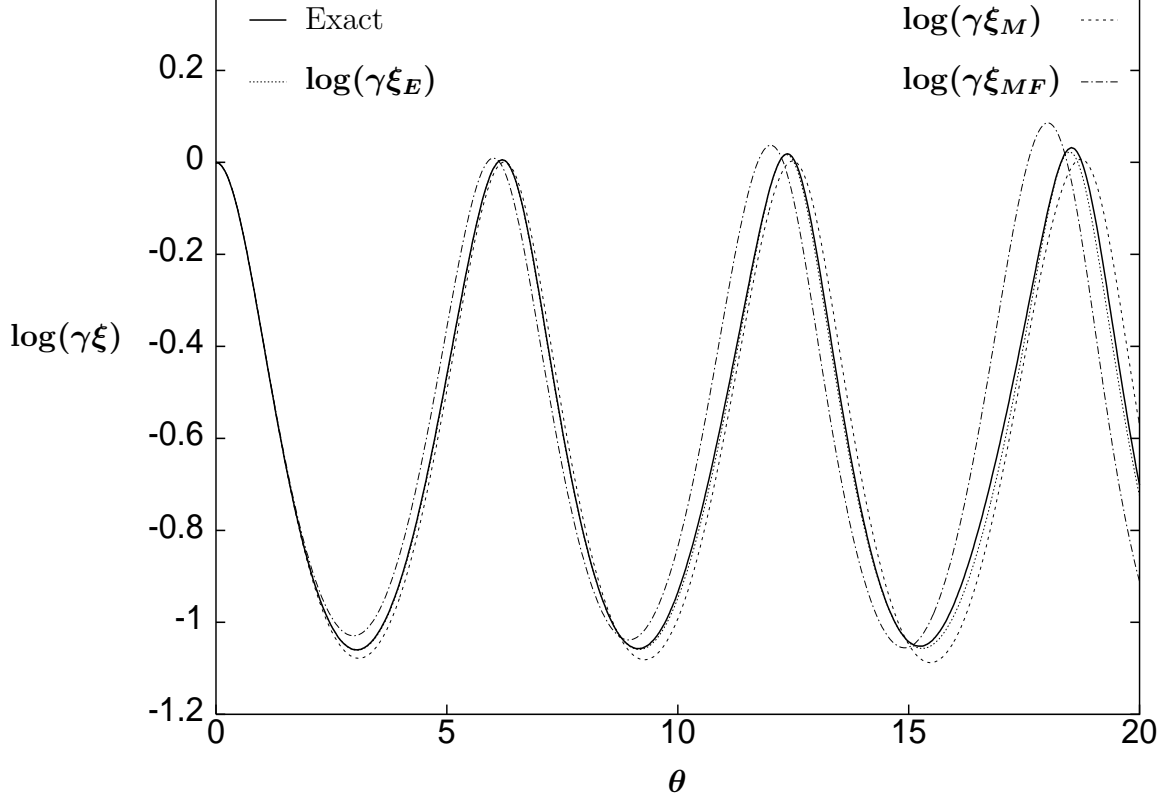
Figure 12: Comparison of $\log(\gamma\xi)$ as a function of θ for various analytical expressions of the correlation as derived in the text. The parameters for all curves are $a = 0.25$, $|\Delta| = 0.5$, $n_b = 0.15$ and $N = 100$. The solid curve is the exact correlation length. In the large N limit all curves overlap completely.

$$q(\langle x \rangle) \approx q(\langle x \rangle + 1/N) \approx q(\langle x \rangle + f/N) \quad , \tag{89}$$

the stationary solution x_0 has a simple parametric representation. To get a consistent expression for the correlation with Eq. (86) the weight factor f has to be

$$f = \frac{a}{2a - 1} \quad . \tag{90}$$

With the approximation Eq. (89), which clearly is very good for large N, Eq. (88) reduces to

$$\frac{1}{\gamma}\frac{d\langle x \rangle}{dt} = -\left[\langle x \rangle - \frac{n_b}{N}\right] + (2a - 1)\, q(\langle x \rangle + f/N) \quad . \tag{91}$$

The stationary solution x_0 of Eq. (91) then satisfies the transcendental mean field equation

$$x_0 = \frac{n_b}{N} + (2a - 1)\, q(x_0 + f/N) \quad . \tag{92}$$

29

In the large N limit, Eq. (92) reduces to Eq. (24) after a multiplication by x_0. In contrast to the saddle-point equation Eq. (24), Eq. (92) therefore always has the trivial $x_0 = 0$ solution in the large N limit. The general solution of Eq. (92) can be written in the following parametric form:

$$x_0(\phi) = \frac{1}{2}\left(-h(\phi) + \sqrt{h^2(\phi) + 4\, g(\phi)}\right) \quad , \tag{93}$$

where

$$h(\phi) \equiv \frac{f - n_b}{N} + \Delta^2 - (2a - 1)\sin^2\phi \quad , \tag{94}$$

$$g(\phi) \equiv \frac{n_b\, f}{N^2} + \Delta^2\frac{n_b}{N} + \frac{f}{N}(2a - 1)\sin^2\phi \quad , \tag{95}$$

and

$$\theta(\phi) = \frac{\phi}{\sqrt{x_0(\phi) + f/N + \Delta^2}} \quad . \tag{96}$$

For small perturbations around x_0, i.e. $\langle x \rangle = x_0 + \delta x$, we find the equation of motion

$$\frac{1}{\gamma}\frac{d\,\delta x}{dt} = -\left[\, 1 - (2a - 1)\, q'(x_0 + f/N)\,\right]\delta x \quad , \tag{97}$$

where

$$q'(x) \equiv \frac{d\,q(x)}{dx} = \frac{\Delta^2}{(x + \Delta^2)^2}\sin^2(\theta\sqrt{x + \Delta^2}) \tag{98}$$

$$+ \frac{x}{(x + \Delta^2)^{3/2}}\,\theta\,\sin(\theta\sqrt{x + \Delta^2})\,\cos(\theta\sqrt{x + \Delta^2}) \quad .$$

In terms of ϕ, Eq. (98) at $x = x_0(\phi)$ reads

$$q'(\phi) = \frac{1}{(x_0(\phi) + f/N + \Delta^2)^2}\left[\,\Delta^2\sin^2\phi + x_0(\phi)\,\phi\sin\phi\cos\phi\,\right] \quad . \tag{99}$$

From Eq. (97) we immediately see that the correlation is given by

$$\gamma\xi \simeq \gamma\xi_{MF}(\phi) = \frac{1}{1 - (2a - 1)\, q'(\phi)} \quad . \tag{100}$$

Notice that $\gamma\xi_{MF}$ is here a function of the parameter ϕ, in contrast to Eq. (75) and Eq. (84).

When the micromaser is not detuned, Eq. (100) reduces to

$$\gamma \xi_{MF}(\phi) = \frac{1}{1 - (2a-1)\dfrac{\phi \sin\phi \cos\phi}{(2a-1)\sin^2\phi + \frac{n_b+f}{N}}} \; . \tag{101}$$

The peak at $\theta = \theta_0^*$ corresponds to

$$\phi = \phi_0^* \approx \left(\frac{3\,(n_b+f)}{N\,(2a-1)} \right)^{1/4} \; . \tag{102}$$

Substituting Eq. (102) into equation Eq. (101) the correlation is

$$\gamma \xi_{MF}(\phi_0^*) = \frac{2a-1}{2} \sqrt{\frac{3\,N}{a + n_b(2a-1)}} \; , \tag{103}$$

for some a the interval $1/2 \le a \le 1$. This correlation is in agreement with Eq. (86).

In the thermal phase, where $x_0 = 0$ in the large N limit, Eq. (100) reduces to

$$\gamma \xi_{MF}(\theta) = \frac{1}{1 - (2a-1)\,\theta_{eff}^2} \; , \tag{104}$$

in agreement with Eq. (76) and Eq. (85).

5.4   Statistical Barrier Penetration

As we have seen above, the correlation length exhibits large peaks for the pump parameters θ_0^*, θ_{kk+1}^* and/or θ_{tk}^*. The correlation grows as $\sqrt{N}$ at $\theta = \theta_0^*$. At θ_{kk+1}^* and θ_{tk}^* the large N dependence is, however, different. At these values of the pump parameter there is instead a competition between two neighbouring minima of the effective potential $V_0(x)$ corresponding to, say, $x = x_0$ and $x = x_2$. A barrier, corresponding to a local maximum of $V_0(x)$ at, say, $x = x_1$, then separates these two minima. Using the technique of [9] it can be shown that the peak in the correlation length close to $\theta = \theta_{kk+1}^*$ is described by the expression

$$\gamma \xi \simeq \frac{2\pi}{\left[\, x_1(1+n_b) + b\,q(x_1)\,\right] \sqrt{-V_0''(x_1)}\; f(x_0, x_1, x_2)} \; , \tag{105}$$

where we have defined

$$f(x_0, x_1, x_2) = \sqrt{V_0''(x_0)}\, e^{-N[V_0(x_1)-V_0(x_0)]} + \sqrt{V_0''(x_2)}\, e^{-N[V_0(x_1)-V_0(x_2)]} \quad . \tag{106}$$

We therefore conclude that

$$\gamma\xi \simeq e^{N\Delta V_0} \quad , \tag{107}$$

where ΔV_0 is the smallest potential barrier between the two competing minima of the effective potential $V_0(x)$. This equation shows explicitly that the correlation length grows exponentially with N. Here we observe that $V_0(\theta)$, and hence also ΔV_0, is proportional to the combination $a + n_b(2a - 1)$ (see Eq. (39)). Since the $\gamma\xi$-peaks grow exponentially with N they cannot be described by Eq. (77) with a finite power expansion of $q(x)$. The first-order transitions at pump parameters corresponding to $\theta = \theta_{tk}^*$ can be treated in a similar fashion.

5.5 Discussion

In Figs. 10, 11 and 12 we show the different analytical expressions for $\gamma\xi$ as given by Eqs. (75), (84) and (100). We have also plotted the exact correlation $\gamma\xi$. For sufficiently large N, all the three expressions are good approximations to the correlation length around the first peak (see Figs. 10 and 11). We also observe that the mean field approximation is a better approximation than Eq. (84). Moreover, the mean field approximation as well as the the assumption $\theta\sqrt{x(\theta) + \Delta^2} \ll 1$ break down for pump parameters beyond the first peak of the correlation length. Hence, neither Eq. (84) nor Eq. (100) is a good approximation for θ's above the first peak (see e.g. Fig. 11). Eq. (100), however, describes some qualitative features of the correlation length also for values of θ above the first peak, even though Eq. (100) then gives numerical values which are quantitatively wrong. We finally notice that all curves in Fig. 12 overlap in the large N limit.

6 TRAPPING STATES

The stationary photon probability distribution Eq. (8) has a special property when $n_b = 0$ and $q_m = 0$. We then have that $\bar{p}_n = 0$ for all $n \geq m$. The cavity then cannot
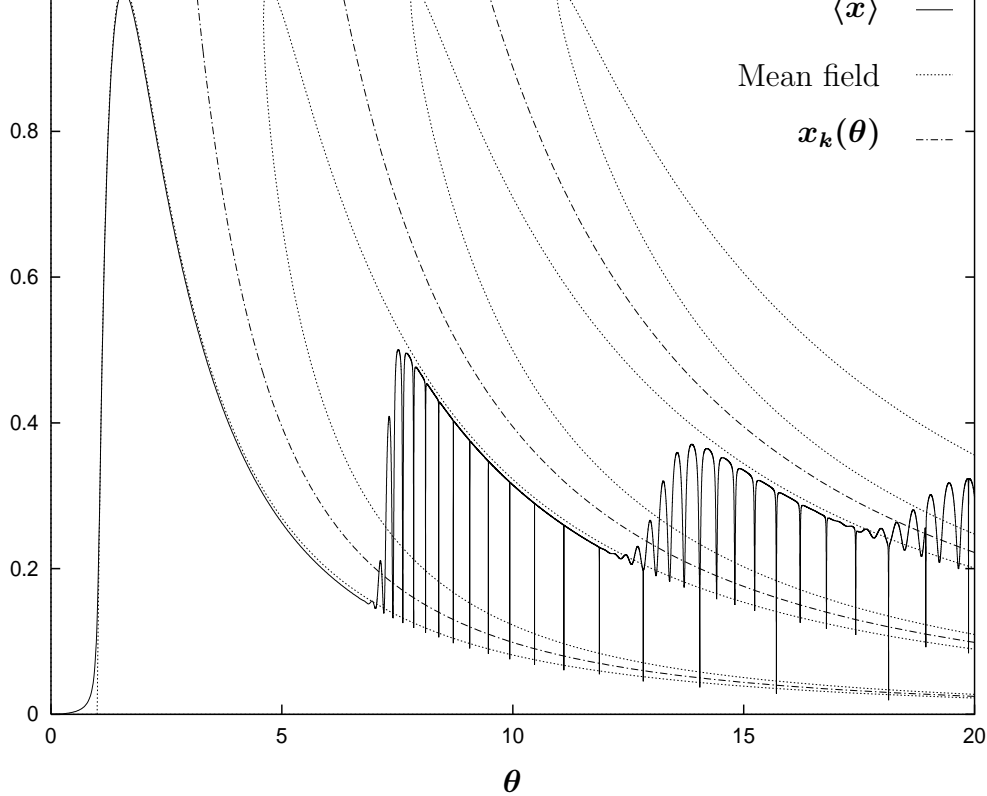
Figure 13: The solid line shows the order parameter $\langle x \rangle = \langle n \rangle / N$ as a function of θ when $n_b = 0$, $a = 1$, $\Delta = 0$ and $N = 100$. As a guide to the eye we have also plotted the mean field solution (see Eq. (26) and Eq. (27)). The dashed-dotted curve is $x_k(\theta)$ (see Eq. (109)). For a given $k \geq 1$, this curve lies between the mean field solutions corresponding to the branches k and $k - 1$.

be pumped above m by photon emission from the pump atoms. The micromaser is then said to be in a trapping state [7, 16]-[19]. Actually, such trapping states have recently been observed in the stationary state of the micromaser system [20]. For a given Δ and $k = 1, 2, 3, ...$, we now define the function

$$\theta_k(x) = \frac{k\pi}{\sqrt{x + \Delta^2}} \quad , \tag{108}$$

or equivalently

$$x_k(\theta) = \frac{(k\pi)^2}{\theta^2} - \Delta^2 \quad . \tag{109}$$

For a given N, trapping states then occur at the pump parameters

$$\theta_{mk}^{tr} = \theta_k(x_{tr}) \quad , \tag{110}$$

where $x_{tr} = m/N$ and $m = 0, 1, 2, 3, ...$.

The effect of trapping states on the order parameter $\langle x \rangle$ is illustrated in Fig. 13 with

an atomic flux parameter $N = 100$. We then clearly observe dips in the order parameter $\langle x \rangle$ due to the presence of trapping states. The observed structure of the dips in $\langle x \rangle$ can be explained as follows. For a given $k \geq 1$, one can prove that the curve described by Eq. (109) lies between the mean field solution corresponding to branch k and $k - 1$ (c.f. Fig. 13). Because of this fact, and since $\langle n \rangle \leq m$, the trapping-dip at θ_{mk}^{tr} reaches down to (in fact, just below) the mean field curve corresponding to branch $k - 1$ (c.f. Fig. 13).

In general, for a given k, trapping states such that the value of m/N is larger than the order parameter $\langle x \rangle$ have a minor effect on the order parameter. When $\theta \lesssim \theta_{01}^*$ (or θ_{t1}^*) the presence of trapping states therefore have little effect on the order parameter (see e.g. Fig. 13) since the curve described by Eq. (109) lies above the order parameter $\langle x \rangle$.

It is easy to realize that trapping effects become less significant when the system is detuned. In this case we see from Eq. (26) and Eq. (109) that $x_k(\theta)$ and the mean field solution is just reduced by the same amount Δ^2. Numerical studies also show that the micromaser phase transitions occur essentially at values of the pump parameter θ almost independent of the value of the detuning $\Delta^2 \leq 1$. Due to these facts the order parameter $\langle x \rangle$, $x_k(\theta)$ in Eq. (109) as well as the mean field solution will intersect with a shifted horizontal θ-axe and hence trapping effects become less important. In passing we notice that, for a given value of the detuning Δ, trapping effects cannot occur for $\theta \leq \theta_{min}^{tr} \equiv \pi/\sqrt{1 + \Delta^2}$. This is due to the fact that the order parameter corresponding to the mean field solution (see Eq. (26) and Eq. (27)) can never exceed unity.

As the atomic flux N increases, the dips in $\langle x \rangle$ due to trapping states become denser as a function of the pump parameter θ [17]. In the large N limit and for $n_b = 0$, $\langle x \rangle$ therefore ceases to be an appropriate order parameter and the system appears to be frustrated. Since the observable $\langle x \rangle$ then varies rapidly it is natural to ask whether it is well defined at all. When the system is in a maser phase and when N is sufficiently large, numerical studies of the standard deviation $\Delta x = \sqrt{\langle x^2 \rangle - \langle x \rangle^2}$ as a function of θ show that Δx is much smaller than the value of $\langle x \rangle$ itself for all possible values of θ, except for values of θ near the phase transitions $\theta = \theta_{kk+1}^*$ and/or $\theta = \theta_{tk}^*$. Hence, the observable $\langle x \rangle$ is actually well defined except near these particular pump parameters.

In Fig. 14 we have studied the correlation length for different values of N. The effect of trapping states becomes more pronounced when N increases. We observe that the peaks in the correlation length corresponding to trapping states get denser for large values of N. Because of the same reasons as discussed earlier in this section, the effect of trapping states on the correlation length become less significant when the system is detuned.

As mentioned in Section 5, the correlation length reaches a maximal value when the

potential barrier between the two competing minima of the effective potential $V_0(x)$ is at its lowest value. If the system is not in a trapping state, the probability distribution $\bar{p}_n$ then essentially consists of two Gaussian peaks with heights which are of the same order of magnitude. Furthermore, due to the pre-factor $w(x)$ in $\bar{p}(x)$ (c.f. Eq. (15)), a micromaser system which is close to a trapping state will also have a probability distribution which essentially consists of two Gaussian peaks of the same order of magnitude, even though the potential barrier between the two competing minima of the effective potential $V_0(x)$ will then be smaller. Hence, the correlation length again reaches a large value. Exactly at a trapping state, however, the probability distribution consists essentially of one dominating Gaussian peak in the large N limit. This means that we should expect the correlation length to become large close to a trapping state however not exactly at the occurence of such a state. Numerical studies are in accordance with these observations. As illustrated in Fig. 15, there is, furthermore, no visible difference between the θ-positions of the peaks of $\gamma\xi$ and the θ-positions of the dips of the $\langle x \rangle$. This is not an obvious fact since ξ measures long-time features of the micromaser system but $\langle x \rangle$ is an instantaneous observable. As the number of branches increases, that is, the number of local maxima in $\bar{p}(x)$ increases, the connection between the heights of the peaks of ξ and the depths of the dips of $\langle x \rangle$ becomes increasingly more complex.

As in Section 5, let λ_n denote the eigenvalues of the matrix L. Introducing the cumulative probability

$$P_n = \sum_{m=0}^{n-1} \bar{p}_n \quad , \tag{111}$$

it was then shown in Ref.[9] that

$$\sum_{n=1}^{\infty} \left(\frac{1}{\lambda_n} - \frac{1}{\lambda_n^0} \right) = \sum_{n=1}^{\infty} \left(\frac{P_n(1-P_n)}{[(1+n_b)n + Nbq_n]\,\bar{p}_n} - \frac{1 - [n_b/(1+n_b)]^n}{n} \right) \quad , \tag{112}$$

where $\lambda_n^0 \simeq n$ is an eigenvalue corresponding to the thermal equilibrium distribution. In the large N limit the left-hand side can be approximated by $\gamma\xi - 1$. Hence, Eq. (112) reads

$$\gamma\xi \approx 1 + \sum_{n=1}^{\infty} \left(\frac{P_n(1-P_n)}{[(1+n_b)n + Nbq_n]\,\bar{p}_n} - \frac{1 - [n_b/(1+n_b)]^n}{n} \right) \quad . \tag{113}$$

When the parameters are as in Fig. 13 we find that, except for a small interval $2 \lesssim \theta \lesssim 4$, the sum-rule prediction Eq. (113) is in surprisingly good agreement with the exact

35
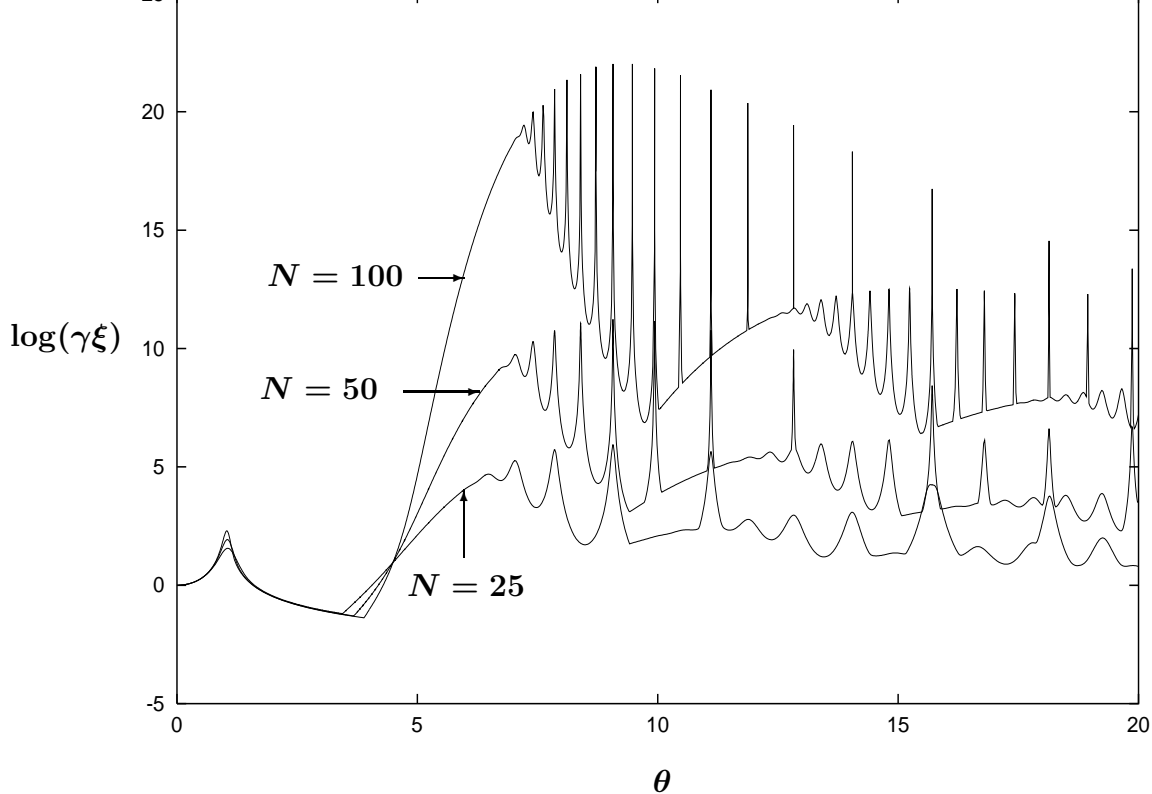
Figure 14: The logarithm of $\gamma\xi$ as a function of θ when $N = 25$, $N = 50$ and $N = 100$ and where $n_b = 0$, $a = 1$ and $\Delta = 0$.

correlation length, even at trapping states. We have no deep explanation of this numerical observation.

7   FINAL REMARKS

We have studied the micromaser phase transitions at non-zero detuning and for pump atoms prepared in a diagonal statistical mixture. New novel features of the micromaser system then emerge as plateaux in the order parameter $\langle x \rangle$ as a function of the atomic density matrix as well as a twinkling behaviour at non-zero detuning. By introducing fluctuations in the pump-parameter θ one can decrease the signal-to-noise ratio in observables like $\mathcal{P}(+)$ and $\mathcal{P}(+, +, t)$ [7, 9, 6]. Elsewhere we will investigate this feature of noise synchronization in more detail, also when the detuning Δ parameter is a random variable. It turns out that fluctuations in Δ also lead to features similar to fluctuations in θ, as was already anticipated in Ref.[7]. Fluctuations in the atomic density matrix parameter a lead, however, not to an output signal of the micromaser with less fluctuations.

36
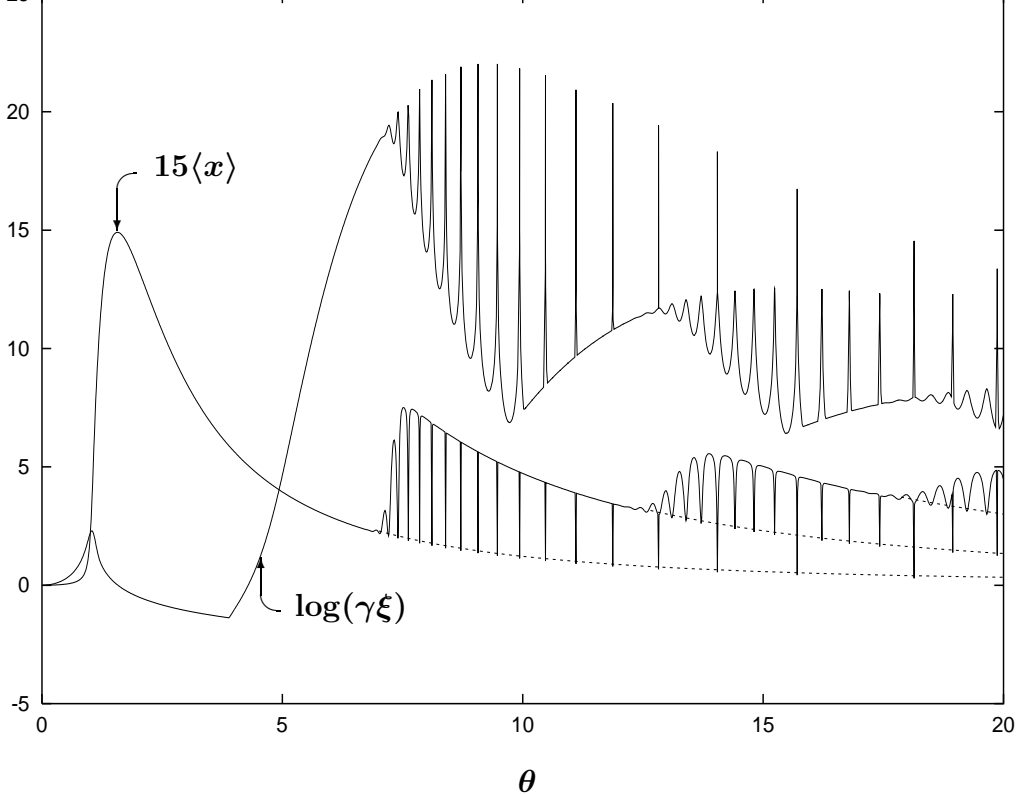
Figure 15: The logarithm of $\gamma\xi$ and $15\langle x\rangle$ as a function of θ when the parameters are as in Fig. 13. There is no visible difference between the θ-positions of the correlation trapping-peaks and the θ-positions of the order parameter trapping-dips. The dotted lines are the mean field solution Eq. (26) and Eq. (27) for branch $k = 0$, $k = 1$ and $k = 2$ for some limited interval of ϕ.

References

[1] H. Walther, "*The Single Atom Maser and the Quantum Electrodynamics in a Cavity* ", Physica Scripta **T23** (1988) 165; "*Experiments on Cavity Quantum Electrodynamics* " Phys. Rep. **219** (1992) 263; "*Experiments With Single Atoms in Cavities and Traps* " in "*Fundamental Problems in Quantum Theory* ", Eds. D. M. Green-

berger and A. Zeilinger, Ann. N.Y. Acad. Sci. **755** (1995) 133; "*Single Atom Experiments in Cavities and Traps*", Proc. Roy. Soc. **A454** (1998) 431; "*Quantum Optics of a Single Atom*", Laser Physics **8** (1998) 1; Physica Scripta **T76** (1998) 138.

[2] K. An, J.J. Childs, R.R. Dasari and M.S. Feld, "*Microlaser: A Laser with One Atom in an Optical Resonator*", Phys. Rev. Lett. **73** (1994) 3375.

[3] L. Caiani, L. Casetti, C. Clementi and M. Pettini, "*Geometry of Dynamics, Lyapunov Exponents, and Phase Transitions*", Phys. Rev. Lett. **79** (1997) 4361; L. Casetti, E.G.D. Cohen and M. Pettini, "*Topological Origin of the Phase Transition in a Mean-Field Model*", Phys. Rev. Lett. **82** (1999) 4160.

[4] A. Buchleitner and R.N. Mantegna, "*Quantum Stochastic Resonance in a Micromaser*", Phys. Rev. Lett. **80** (1998) 3932.

[5] A. Maritan and J.R. Banavar, "*Chaos, Noise, and Synchronization*", Phys. Rev. Lett. **72** (1994) 1451.

[6] B.-S. Skagerstam in "*Applied Field Theory*", Eds. Choonkyu Lee, Hyunsoo Min and Q-Han Park (Chungbum Publ. House, Seoul, 1999).

[7] D. Filipowicz, J. Javanainen and P. Meystre, "*The Microscopic Maser*", Opt. Comm. **58** (1986) 327; "*Theory of a Microscopic Maser*" Phys. Rev. **A34** (1986) 3077.

[8] A.M. Guzman, P. Meystre and E. M. Wright, "*Semiclassical Theory of the Micromaser*", Phys. Rev. **A40** (1989) 2471.

[9] P. Elmfors, B. Lautrup and B.-S. Skagerstam, "*Correlations as a Handle on the Quantum State of the Micromaser*", CERN/TH 95-154 (cond-mat/9506058); Physica Scripta **55** (1997) 724; "*Correlations in the Micromaser*" Phys. Rev. **A54** (1996) 5171.

[10] O. Benson, G. Raithel and H. Walther, "*Quantum Jumps of the Micromaser Field: Dynamic Behavior Close to Phase Transition Points*", Phys. Rev. Lett.**72** (1994) 3506 and "*Dynamics of the MicroMaser Field*" in "*Electron Theory and Quantum Electrodynamics: 100 Years Later*", Ed. J.P. Dowling (Plenum Press, New York, 1997).

[11] P.K. Rekdal and B.-S. Skagerstam, *"On the Phase Structure of the Micromaser "*, Trondheim Seminar in Theoretical Physics **4** (1999) and quant-ph/9910110 (submitted for publication).

[12] L. Lugiato, M. Scully and H. Walther, *"Connection Between Microscopic and Macroscopic Maser Theory "*, Phys. Rev. **A36** (1987) 740.

[13] M.O. Scully and M.S. Zubairy, *"Quantum Optics "* (Cambridge University Press, Cambridge, 1996).

[14] E.T. Jaynes and F.W. Cummings, *"Comparison of Quantum and Semiclassical Radiation Theories with Application to the Beam Maser "*, Proc. IEEE **51** (1963) 89.

[15] See e.g. R. Courant and D. Hilbert, *"Methods of Mathematical Physics "* (Interscience, New York, 1953) and M. Fleischhauer and W.P. Schleich, *"Revivals Made Simple: Poisson Summation Formula as a Key to the Revivals in the Jaynes-Cummings Model* , Phys. Rev. **A47** (1993) 4258.

[16] P. Filipowicz, J. Javanainen and P.Meystre, *"Quantum and Semiclassical Steady States of a Kicked Cavity Mode "*, J. Opt. Soc. Am. B **3** (1986) 906.

[17] P. Meystre, G. Rempe and H. Walther, *"Very-Low-Temperature Behavior of a Micromaser "*, Opt. Lett. **13** (1988) 1078.

[18] P. Meystre and J.J. Slosser, *"Destruction of Quantum Coherence in a Micromaser by Finite Detection Efficiency "*, Opt. Comm. **70** (1989) 103.

[19] J.J. Slosser and P. Meystre *"Tangent and Cotangent States of the Electromagnetic Field "*, Phys. Rev. A **41** (1990) 3867.

[20] M. Weidinger, B.T.H. Varcoe, R. Heerlein and H. Walther, *"Trapping States in the Micromaser "*, Phys. Rev. Lett. **82** (1999) 3795.

[21] G. Rempe, H. Walther and N. Klein, *"Observation of Quantum Collapse and Revival in the One-Atom Maser "*, Phys. Rev. Lett. **58** (1987) 353.

[22] M. Brune, F. Schmidt-Kaler, A. Maali, J. Dreyer, E. Hagley, J.M. Raimond and S. Haroche, *"Quantum Rabi Oscillation: A Direct Test of Field Quantization in a Cavity "*, Phys. Rev. Lett. **76** (1996) 1800.